NASA CONTRACTOR REPORT 158904

AERODYNAMIC CHARACTERISTICS OF A JET SHEET VORTEX GENERATOR

by H. Ziegler and P. T. Wooler

Prepared by
NORTHROP CORPORATION, AIRCRAFT GROUP
Hawthorne, California
for Langley Research Center

NATIONAL AERONAUTICS AND SPACE ADMINISTRATION • WASHINGTON, D.C. • JUNE 1978

Aerodynamic Characteristics of a Jet Sheet Vortex Generator

H. Ziegler and P. T. Wooler

Prepared under Contract No. NAS 1-14216 by
NORTHROP CORPORATION, AIRCRAFT GROUP
Hawthorne, California

for Langley Research Center

NATIONAL AERONAUTICS AND SPACE ADMINISTRATION

FOREWORD

This report presents a summary of work performed as part of a joint Northrop-NASA study of the concept of lift augmentation due to the vortex flow from a jet sheet formed by blowing from a series of in-line orifices located in the side of the fuselage ahead of the wing.

The high-speed test of this investigation was conducted in the Langley 7-by 10-foot high-speed wind tunnel. The authors wish to thank Messrs. Jarrett K. Huffman and Charles H. Fox, Jr., for their valuable contributions to that effort.

The work was performed under the technical cognizance of Dr. James F. Campbell, whose interest in, and support of, this study are gratefully acknowledged.

This report has been assigned the Northrop report number NOR 78-24, for internal control purposes.

CONTENTS

AERODYNAMIC CHARACTERISTICS OF A JET SHEET VORTEX GENERATOR

by H. Ziegler and P. T. Wooler
Northrop Corporation, Aircraft Group
Hawthorne, California

SUMMARY

A new configuration concept for augmenting the lift capability of low aspect ratio, thin wings, typically used on fighter aircraft, has been investigated. The fluid strake concept uses a jet sheet formed by blowing from a series of small in-line orifices located in the side of the fuselage ahead of the wing to generate a stable vortex flow over the wing at high angle of attack.

A half-span model designed to demonstrate the concept was tested in the Northrop 7- by 10-foot low-speed tunnel. The effect of location of the fluid strake relative to the wing was investigated for three different designs of the in-line orifices generating the jet sheet. Two wings of differing leading edge sweep were employed to determine the influence of this parameter on the effectiveness of the concept as a lift-augmenting device. With proper positioning relative to the wing, the fluid strake generated significant increases in lift at high angle of attack and improved drag polars. Lift increments were strongly dependent on the jet momentum coefficient.

Based on the results of the low-speed test, a jet-sheet producing module was designed for incorporation into a NASA general research fighter model and tested in the Langley 7- by 10-foot high-speed tunnel to determine the effectiveness of the fluid strake as a lift-enhancement device in the high-speed maneuver regime. Tests were conducted over a Mach number range from 0.3 to 0.8, with a jet momentum coefficient range from 0 to 0.24. Again, significant lift increments resulted at the higher angles of attack and drag polars were improved. The effectiveness of the fluid strake as a lift-generator was essentially independent of Mach number within the range tested. Improvements in longitudinal aerodynamic characteristics were achieved without adversely affecting lateral directional stability. The vertical tail effectiveness was improved by the vortex flow and loss of directional stability was delayed to higher angle of attack.

The lift augmentation due to operating the fluid strake was generally comparable to that generated by other propulsive devices, such as spanwise blowing.

Integration of the fluid strake into a fighter aircraft design, by considering the impact of its power requirements on the main-engine thrust, shows a payoff in specific excess power available for maneuvering at higher load factors.

INTRODUCTION

Modern tactical fighter aircraft design involves the conflicting objectives of efficient supersonic performance and maneuvering capability in the subsonic and transonic regimes. The low aspect ratio, thin wings designed for supersonic performance are not conducive to developing the high lift coefficients at low drag required for subsonic and transonic maneuvering. The primary measure of maneuverability is the turn rate which is governed by the amount of excess lift which can be generated for a given set of flight conditions. Thus, to increase the maximum lift capability of moderately swept, thin wings, a number of aerodynamic design concepts have been developed that take advantage of the strong leading edge vortex which is shed from thin slender wings and strakes at angle of attack.

It is shown in Reference 1 that, for slender wings, the vortex bursting point moves forward from the trailing edge as the angle of attack is increased. Thin wings with moderate leading edge sweep experience vortex bursting at low angles of attack so that vortex-induced effects are essentially nonexistent for such wings.

One method for achieving the desired vortex flow is to use a sharp-edged highly swept strake (or leading edge extension). The vortex, in turn, produces favorable flow over the wing, resulting in increased lift at high angle of attack and, for a given lift, reduction of drag at high lift (Reference 2).

Another technique that has received research attention consists of blowing a concentrated jet over the wing's upper surface in a direction essentially parallel to the wing leading edge. This enhances the leading edge vortex on moderately swept wings and effectively delays vortex breakdown to higher angles of attack (References 3-5).

A new method for inducing favorable vortex flow over the wing is investigated here. The jet sheet vortex generator concept, illustrated in the following sketch, uses a jet sheet formed by blowing from a series of in-line orifices located in the side of the fuselage forward of the wing. The jet sheet will have a vorticity distribution associated with it and will induce a stable vortex flow about the jet sheet, similar to the vortex generated by a strake. In view of this similarity, and in an effort to simplify the terminology, the jet sheet vortex generator will be referred to as a fluid strake.

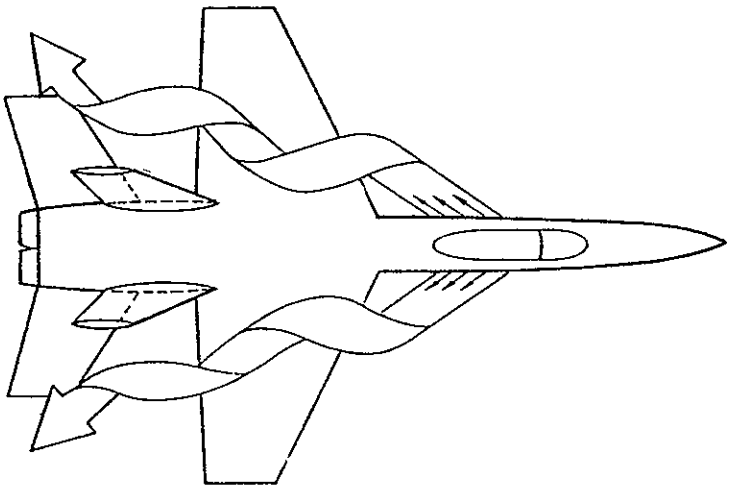

Sketch 1. Schematic of Fluid Strake Concept

Results from tests of the spanwise blowing concept showed that, in order to substantially augment the lift, blowing requirements were quite large at the high subsonic speeds typical of fighter maneuver conditions. The fluid strake concept was based on the reasoning that if the jet sheet were located ahead of the wing its deflection angle relative to the fuselage axis could be smaller. This would result in a larger component in the thrust direction, i.e., being effectively recovered as thrust. The thrust-loss penalty at the higher blowing rates would, consequently, not be as severe.

The investigation described here was conducted in two phases, to determine the effectiveness of the fluid strake as a lift-enhancement device at high angle of attack in both low-speed and high-speed regimes. A half-span model designed to demonstrate the concept was tested in the Northrop 7- by 10-foot low-speed tunnel. The effect of location of the fluid strake relative to the wing was investigated for three different designs of the in-line orifices generating the jet sheet. Two wings of differing leading edge sweep were employed to determine the influence of this parameter on the effectiveness of the concept as a lift-augmenting device. Details of this phase of the investigation are given in Part 1 of this report.

Based on the results of the low-speed test, a jet-sheet producing module was designed for incorporation into a NASA general research fighter model to determine the effectiveness of the fluid strake as a lift-enhancement device in the high-speed maneuver regime. The wind tunnel tests were performed in the Langley 7- by 10-foot high-speed tunnel at Mach numbers up to 0.8. Details of this wind tunnel investigation have been reported in Reference 6. Analyses of the data from that study are presented in Part 2 of this report.

SYMBOLS

A_e	total orifice exit area
b	wing span
C_D	aerodynamic drag coefficient, corrected for thrust from fluid strake
C_L	aerodynamic lift coefficient, corrected for thrust from fluid strake
ΔC_L	lift increment due to fluid strake, jet-on lift minus jet-off lift
$C_{L,o}$	aerodynamic lift coefficient without fluid strake
$C_{L,p}$	potential lift coefficient
$C_{L,tot}$	sum of potential and vortex lift coefficients
C_ℓ	aerodynamic rolling moment coefficient, Rolling moment/qSb
C_{ℓ_β}	rolling moment due to sideslip, $\partial C_\ell / \partial \beta$, per deg (between +5° and -5° in β)
$C_{\ell_{\beta VT}}$	effective dihedral due to vertical tail, C_{ℓ_β} (tail on) - C_{ℓ_β} (tail off)
C_n	aerodynamic yawing moment coefficient, Yawing moment/qSb
C_{n_β}	yawing moment due to sideslip, $\partial C_n / \partial \beta$, per deg (between +5° and -5° in β)
$C_{n_{\beta VT}}$	vertical tail effectiveness, C_{n_β} (tail on) - C_{n_β} (tail off)
C_μ	jet momentum coefficient, $\dot{\omega} V_j / gqS$
$\bar{c}$	wing mean aerodynamic chord
D	aerodynamic drag
d	orifice diameter
ϵ	roughness value for circular orifices
F_x	axial force
F_y	side force
F_z	normal force
g	gravitational acceleration
L	aerodynamic lift
ℓ	orifice length
M	freestream Mach number
p	freestream static pressure
$p_{t,p}$	stagnation pressure in plenum
q	freestream dynamic pressure

SYMBOLS (Continued)

S	wing reference area
s	spacing between circular orifices
T	engine thrust
$T_{t,p}$	stagnation temperature in plenum
V_j	jet velocity due to isentropic expansion to freestream static pressure
V	freestream velocity
W	aircraft weight
$\dot{\omega}$	air weight flow rate
α	angle of attack, deg
β	angle of sideslip, deg
θ	fluid strake deflection angle } see Figure 2.5
ϕ	fluid strake declination angle } see Figure 2.5

Model Nomenclature

Part 1:

D1, D2, D3, D4, D5	locations of fluid strake relative to wing, defined in Figure 1.4
P1, P2, P3	plenum-cover plate combinations to generate jet sheet (see Figure 1.3)
W1	26°-swept wing } see Figure 1.2
W2	50°-swept wing } see Figure 1.2

Part 2:

H	horizontal tail
N1	aft nozzle configuration } see Figure 2.1
N2	forward nozzle configuration } see Figure 2.1
W1	mid-wing } see Figure 2.1
W2	low-wing } see Figure 2.1

PART 1: HALF-SPAN MODEL TEST

A half-span model, designed to demonstrate the concept of lift enhancement at high angle of attack due to the vortex flow generated by a fluid strake, was tested in the Northrop 7- by 10-foot low-speed tunnel. The effect of location of the fluid strake relative to the wing was investigated for three different designs of the in-line orifices generating the jet sheet. Two wings of differing leading edge sweep were utilized to establish the influence of this parameter on the effectiveness of the fluid strake as a lift-augmenting device.

DESCRIPTION OF MODEL

The model used for the test was a half-span arrangement using a left wing mounted above a splitter plate on the tunnel floor as shown in Figure 1.1(a). High pressure air was supplied to the plenum from a 3000 psi high pressure storage system. Details of the plenum mounted below the splitter plate may be seen in Figure 1.1(b). A number of cover plates and inserts which fit on top of the plenum and flush with the upper surface of the splitter plate were employed to vary the location of the orifices generating the jet sheet with respect to the wing.

Two different wings, typical of the low aspect ratio thin wings utilized in fighter design, were used for the test: (1) an uncambered and untwisted wing with an aspect ratio of 3.32, a taper ratio of 0.372, based on the root chord, and a leading edge sweep of 26.7°; (2) an uncambered and untwisted cropped delta wing with an aspect ratio of 2.03, a taper ratio of 0.20, based on the root chord, and a leading edge sweep of 50°. In the streamwise direction both wings have a rectangular section beveled to a sharp leading and trailing edge. They are shown in Figure 1.2 and are designated W1 and W2, respectively.

The cover plates used in combination with the plenum to generate the jet sheet utilized two slot designs and a series of in-line circular holes as orifices as shown in Figure 1.3. The first design (designated P1) is a slot 28.4 cm (11.18 in.) long and 0.0254 cm (0.01 in.) wide with a taper angle of 16° to converge the flow through the plate 0.635 cm (0.25 in.) thick. Vanes 0.05 cm (0.02 in.) thick are spaced 1.0 cm

(0.4 in.) apart to direct the flow at 20° to the model axis. The other slot design (P2) differed only in plate thickness, i.e., slot depth and vane length, as shown in Figure 1.3. By adding the extra constant-width channeling section the flow angularity is expected to be more uniform and closer to the design goal of 20°. However, the additional channel with a length-to-width ratio of ≈73 will lead to greater total pressure losses and result in a lower nozzle efficiency for the design.

The third cover plate (P3) utilizes a series of 31 holes of 0.10 cm (0.04 in.) diameter, spaced at 0.41 cm (0.16 in.) to generate the jet sheet. The holes are drilled at an angle of 30° to the model axis. The possibility of obtaining two-dimensional jet flow from a series of closely spaced uniform holes in line has been investigated both theoretically and experimentally in Reference 7. The data of Reference 7 show that fully merged two-dimensional flow occurs at approximately twelve hole diameters downstream of the exit plane, with the actual distance being a function of the hole spacing, s/d. With the data of Reference 7 to serve as a guide for spacing the holes, it was felt that this design, (P3), would reduce the complexity of fabricating the jet-sheet producing module for the high-speed test.

Combinations of these cover plates and inserts for the splitter plate allowed the jet sheet to be generated at the various locations relative to the wing shown in Figure 1.4. The nomenclature of Figure 1.4 is used to identify the relative location of the fluid strake with respect to the wing in the discussion which follows.

The 26°-swept wing (W1) was also tested in combination with a highly swept strake immediately ahead of the wing and in the plane of the wing. The strake had a leading edge sweep of 72° and an exposed area of 6% of the wing area.

APPARATUS, TESTS AND CORRECTIONS

The wing was mounted to a six-component force balance beneath the splitter plate. The plenum was equipped with three static pressure taps and one thermocouple. Air weight flow through the plenum was measured using a 1.27 cm (0.5 in.) diameter orifice meter installed in a 4.06 cm (1.6 in.) diameter pressure line.

The jet momentum coefficient, C_μ, is defined as $\dot{\omega}V_j/gqS$ where $\dot{\omega}$ is the weight flow rate through the plenum and V_j is the jet velocity reached by isentropic expansion from the stagnation pressure at the orifice exit to free-stream static pressure. Taking the ratio of specific heats for air to be 1.40, yields

$$V_j = 109.6 \sqrt{T_{t,p} \left\{1 - \left(\frac{p}{p_{t,p}}\right)^{\frac{2}{7}}\right\}} \qquad (1.1)$$

in ft/sec with the plenum total temperature in °R. By using the plenum total pressure in Eq (1.1), the ideal jet momentum coefficient is considered, i.e., total pressure losses through the orifices are neglected in computing V_j. However, the weight flow rate, which for choked flow is a linear function of the total pressure at the orifice exit, is a measured parameter. Thus, the major effect of total pressure losses through the orifices on C_μ is accounted for.

Since the jet momentum coefficient varied slightly during a given test run, a nominal jet momentum coefficient, corresponding to the preset tunnel dynamic pressure, plenum total pressure and average plenum total temperature was computed. This term is designated C_μ and is used to identify the data. The range of C_μ for a given configuration was obtained by presetting the plenum total pressure and varying the tunnel dynamic pressure.

Tests were made at tunnel dynamic pressures ranging from 5 to 50 psf. Plenum total pressures ranged from 70 to 120 psia. A run consisted of pitching the wing (yawing the splitter plate on the turntable) through an angle of attack range from -5° to 40° in increments of 5°.

The wing angle of attack was corrected for deflection of the balance and sting support system due to aerodynamic load. Since the wing was the only metric portion of the model, no corrections of the aerodynamic data for thrust effects due to the jet sheet were required.

RESULTS AND DISCUSSION

Plenum Calibration

The various plenum-cover plate combinations (P1, P2, P3) were pressurized and attempts to approximate the flow angularity of the jets emanating from the orifices were made with tuft studies. For P1, the vane spacing and nozzle contraction resulted in a jet sheet with a deflection of approximately 40° to the model axis. With the extra length of guide vanes in the constant-width channel of P2, the flow angularity improved to approximately 30°. The flow angularity of P3 was found to be somewhat greater than the 30° design value. For P2 and P3, asymmetric expansion of the flow at the orifice exit,

due to the fact that the nozzles do not emerge at 90° to the surface of the cover plates, leads to flow deflection angles of the jet sheet which are larger than the design values of 20° and 30°, respectively.

Figure 1.5 shows weight flow rates measured for P1, P2, P3 as a function of plenum total pressure. Also shown are curves of maximum theoretical weight flow rates (choked conditions) corresponding to maximum and minimum slot exit area for P1 and P2. Exit area is computed as the area normal to the assumed flow direction, as shown below.

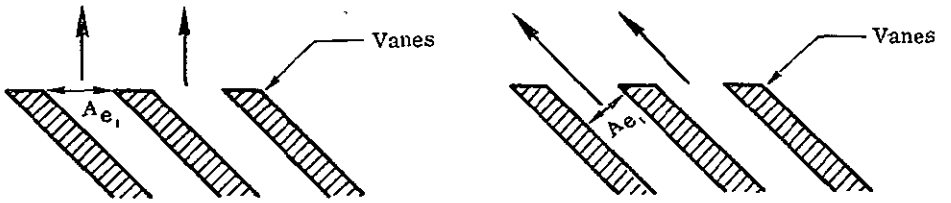

(a) (b)

Sketch 2. Maximum and Minimum Exit Areas

Maximum exit area, as shown in (a), occurs if there is no turning of the flow due to the vanes and the air exits normally to the model axis. Then,

$$A_{e\,max} = (28.4)(.0254) - 27(.05)(.0254)/\sin 20°$$
$$= 0.62 \text{ cm}^2$$

Minimum exit area, depicted in (b), occurs when the flow is fully aligned by the vanes,

$$A_{e\,min} = (28.4)(.0254)\sin 20° - 27(.05)(.0254)$$
$$= 0.21 \text{ cm}^2$$

The maximum theoretical weight flow rate for P3 is based on the total area for the 31 circular orifices,

$$A_e = 31(\pi/4)(.10)^2$$
$$= 0.24 \text{ cm}^2$$

All computations are based on zero pressure losses. The measured weight flow rates are all consistently high when compared to maximum theoretical weight flow rates.

The measured weight flow rate for P1 is seen to be close to the maximum theoretical weight flow rate based on a maximum exit area. A flow deflection angle of 40° was observed for P1 (indicating that the exit area was reduced) and some pressure losses would be expected also. The measured weight flow rate for P2 is seen to be close

to the maximum theoretical weight flow rate based on the minimum exit area. This shows the right trend, in that the flow deflection angle for P2 was observed to be closer to the design value due to the longer vanes. However, the large total pressure losses expected for this configuration, due to the constant-width channel with high length-to-width ratio, are not reflected in the measured weight flow rate. The measured weight flow rate for P3 is approximately 95% of the maximum theoretical weight flow rate based on the plenum total pressure. For P3, total pressure loss predictions based on ℓ/d of the individual orifices of 12.5, are in the range of 20% to 25%, corresponding to a range of assumed roughness values ($.0001 \leq \epsilon \leq .001$) for the drilled holes. Thus, the measured weight flow rate for P3 is seen to be high on the order of 20%.

Since repeated leak checks performed during the test for all three plenum-cover plate combinations failed to show any problems in this respect (and weight flow rate measurements showed good repeatability) it was concluded that the problem was in the weight flow meter. The jet momentum coefficients for the half-span test are all based on the measured weight flow rates, with no attempt to correct them for the suspected error in the instrumentation.

Flow Visualization

Flow visualization runs employing smoke probes near the orifices producing the fluid strake showed that, at high angle of attack, the freestream interaction with the jet sheet produced a streamwise vortex, similar to the vortex generated by a physical strake. The streamwise vortex, in turn, produces favorable flow gradients over the wing, inducing outwash over the wing and keeping the flow from separating.

Oil flow photographs for the 26°-swept wing are shown in Figure 1.6. With blowing on, an increased region of attached flow with a large component of velocity in the wingtip direction may be identified.

Force Data

The effect of the fluid strake on the aerodynamic characteristics of each of the two wings tested is shown in Figures 1.7 to 1.13. Generally, the data indicate that, with proper location of the fluid strake relative to the wing, the interaction of the freestream with the jet sheet generates a vortex flow over the wing, increasing $C_{L_{max}}$ as well as the angle of attack at which $C_{L_{max}}$ occurs and improving the drag polars at high C_L. A more detailed discussion of the results presented in these figures follows.

Effect of Horizontal Displacement of Fluid Strake. The effect of horizontal displacement of the fluid strake relative to the wing is shown for W1 in Figure 1.7. The jet sheet is formed in the plane of the wing at positions D1 and D2 as defined in Figure 1.4. For the same jet momentum coefficients, similar improvements in aerodynamic characteristics are observed for both locations of the fluid strake. $C_{L_{max}}$ is increased approximately 25%. Jet sheet location D2 is slightly more effective in improving C_L up to $\alpha = 20°$, whereas displacing the jet sheet horizontally to location D1 is seen to be more effective in improving lift characteristics at $\alpha > 25°$. Within the limited range tested, horizontal displacement of the fluid strake does not have a significant effect on its performance as a lift-enhancement device.

Effect of Vertical Displacement of Fluid Strake. The effect of vertical displacement of the fluid strake relative to the wing is shown in Figures 1.8 and 1.9 for W1 and W2, respectively. From Figure 1.8, it is apparent that vertical displacement of the jet sheet above the plane of the wing causes the beneficial effects of the induced vortex flow to diminish rapidly. No improvement in aerodynamic characteristics is obtained by placing the jet sheet at locations D3 and D4 above the wing. The in-line position D2 is seen to be the most effective location for the fluid strake. The same trends may be seen in Figure 1.9, where the effect of vertical displacement of the fluid strake on the lift of W2 is shown.

Position D5 would appear to be favorable since the leading edge location of the jet sheet in this position causes the vortex to pass closest to the wing's upper surface. However, the effectiveness of the fluid strake in this position may be diminished due to flow generated at the trailing edge of the jet sheet impinging on the bottom surface of the wing.

Comparisons between Figure 1.8 and 1.9 also show that the leading edge sweep angle of the wing does not have a significant impact on the effectiveness of the fluid strake as a lift-augmenting device. Although Figures 1.8 and 1.9 do not isolate the effects of wing sweep since different fluid strake locations are used with the two wings, it can be observed that the primary effect of increased leading edge sweep is to delay the lift-increments due to the fluid strake to higher angle of attack. This is, of course, related to the amount of vortex flow on the wing before implementation of the fluid strake. For the bare 26°-swept wing, vortex-induced effects are essentially nonexistent so that the effects of the vortex flow due to the fluid strake become evident at $\alpha = 12°$ to 14°. For the 50°-swept wing, on which some vortex lift already exists, the effects of

the jet-sheet induced vortex flow do not become significant until $\alpha = 20°$. In terms of lift enhancement, increments in $C_{L_{max}}$ per unit C_μ are seen to be comparable for both wings.

Effect of Orifice Shape and Jet Momentum Coefficient. The effects of jet momentum coefficient and type of orifice utilized to form the jet sheet are shown in Figures 1.10 through 1.12. From Figure 1.10 it can be shown that the type of orifice used for forming the jet sheet does not have a major effect on the improvement in lift capability achieved for W1. P2 represents the least effective manner of generating the jet sheet (in terms of an augmentation ratio $\Delta C_{L_{max}}/C_\mu$) of the three configurations shown.

Figure 1.11 shows the effects of jet momentum coefficient and nozzle type on the lift enhancement achieved for W2. Again, lift increments achieved correlate primarily with jet momentum coefficient, without major influence by the manner in which the jet sheet is formed.

The effect of concentrating the jet sheet (i.e., achieving the same jet momentum coefficient while reducing the number of orifices used to form the fluid strake) is shown in Figure 1.12. Plenum-cover plate combination $P2_b$ is P2 with 32% of the forward extent and 21% of the aft extent of the slot blocked off. Thus, the same C_μ is generated by increased weight flow through a reduced length, resulting in a more concentrated jet sheet. The data show that $P2_b$ results in lift augmentation which is virtually identical to the lift augmentation generated by P2, up to 25° angle of attack. At angles of attack larger than 25°, the longer jet sheet emanating from P2 is seen to be slightly more effective. It should be noted that a switch from P2 to $P2_b$ involves a horizontal displacement of the jet sheet as well as a change in the concentration.

Comparison with Physical Strake. Figure 1.13 shows a comparison of the improvement in aerodynamic performance of W1 due to the fluid strake with that due to another lift-enhancement device, a highly swept strake immediately ahead of the wing and in the plane of the wing. A jet sheet with $C_\mu = 0.20$ gives superior lift and drag benefits at the moderate to high angles of attack. The significant increases in lift and drag improvements which can be realized with increasing C_μ are also illustrated by including data for $C_\mu = 0.44$. These significant improvements which can be realized for high blowing rates must, of course, be viewed in light of the power demands posed by such high blowing rates. This point will be dealt with in more detail in Part 2 of this study, where power tradeoff data for complete, although assumed, aircraft configurations are presented.

CONCLUSIONS

A half-span model, designed to demonstrate the concept of lift enhancement at high angle of attack due to the vortex flow generated by a fluid strake, was tested. Effects of jet sheet location relative to the wing, wing leading edge sweep, and type of orifice utilized to generate the jet sheet were investigated to establish guidelines for designing a jet-sheet producing module for testing in the high-speed maneuver regime. As a result of this study the following conclusions were formed:

- A jet sheet formed by blowing from a series of small in-line orifices in the side of the fuselage ahead of the wing can be an effective lift-enhancing device at high angle of attack by generating a favorable vortex flow over the wing. This results in increased $C_{L_{max}}$, a higher angle of attack at which $C_{L_{max}}$ occurs, and improved drag polars at high C_L.
- The performance of the fluid strake as a lift-enhancement device is a strong function of the jet momentum coefficient. At high blowing rates, the significant improvements in aerodynamic performance must be viewed in light of the power demands posed by such blowing rates.
- Vertical displacement of the fluid strake with respect to the wing has a significant impact on its effectiveness as a lift-enhancement device. Incremental lift due to the induced vortex flow diminishes drastically with increasing displacement of the fluid strake above the plane of the wing. For maximum effect, the vortex should pass close to the upper surface of the wing, without impingement of flow from the trailing edge of the jet sheet on the lower surface of the wing.
- Horizontal displacement of the jet sheet relative to the wing did not have a significant effect on the improvement of lift on the wing, within the limited range tested.
- The type of orifice used to form the jet sheet did not have a major effect on the benefits in performance derived from the induced vortex flow. The length of the fluid strake was also not an important parameter.
- Wing leading edge sweep did not significantly affect the performance of the fluid strake as a lift-enhancement device. Increased leading edge sweep delayed the lift increments due to the fluid strake to higher angle of attack.

PART 2: HIGH-SPEED TEST

Based on the results of Part 1, a jet-sheet generating module was designed for incorporation into a general research fighter model to investigate the fluid strake as a lift-enhancement device in the high-speed maneuver regime. Tests were conducted in the Langley 7- by 10-foot high-speed tunnel over a Mach number range of 0.3 to 0.8. Four different locations of the fluid strake with respect to the wing were investigated. Details of this wind tunnel study have been reported in Reference 6.

DESCRIPTION OF MODEL

Geometry details of the general research model are presented in Figure 2.1. Photographs of the model installed in the tunnel are shown in Figure 2.2. The basic model consisted of a simple wing-fuselage-vertical tail combination. The uncambered and untwisted wing had an aspect ratio of 2.50 and a taper ratio of 0.20 based on the theoretical root chord, a leading edge sweep of 44° and a NACA 64A series airfoil section in the streamwise direction with a thickness ratio of 6% at the fuselage juncture and 4% at the wingtip. The wing height was varied as shown in Figure 2.1, so that the arrangement represented either a mid-wing or a low-wing configuration. The vertical displacement of the fluid strake with respect to the wing was effected in this manner.

The lower forward portion of the fuselage contained the jet-sheet producing module, consisting of the model air supply plenum and twenty individual nozzle orifices of 0.16 cm (0.063 in.) diameter, inclined at 30° to the model axis, on each side of the fuselage (see Figures 2.1 and 2.2). The plenum was connected to the 7- by 10-foot high-speed tunnel low mass flow balance air fixture, and the high pressure air was delivered through the 7- by 10-foot high-speed tunnel air sting.

The longitudinal displacement of the fluid strake was accomplished by selectively blocking off groups of orifices inside the plenum. A set of 10 contiguous orifices on each side was utilized to form the jet sheet with a length of 5.72 cm (2.25 in.).

The single centerline-mounted uncambered and untwisted vertical tail had a sharp leading edge with a sweep angle of 51.7° and an exposed area of 12.5% of the wing area. One configuration employed an uncambered and untwisted horizontal tail which had a

sharp leading edge with a sweep angle of 51.7° and an exposed area of 25% of the wing area. The horizontal and vertical tails had a circular arc airfoil section with a thickness ratio of 6% at the fuselage juncture and 4% at the tip.

APPARATUS, TESTS AND CORRECTIONS

Six-component force and moment data were measured by means of an internally mounted strain-gage balance. High pressure air was delivered across this balance to the model plenum by means of two S-shaped tubes. The calibration of this balance has demonstrated that the air crossing the balance does not affect any component except axial force. The effect on axial force is a tare effect which is a linear function of the plenum pressure.

A pressure probe and thermocouple were used to monitor plenum stagnation pressure and temperature. These data were used to calculate the balance axial force pressure tare and the jet velocity.

The air weight flow rate was determined by means of a calibrated venturi type flow meter located in the main air supply line. The jet momentum coefficient is again defined as $\dot{\omega}V_j/gqS$ where $\dot{\omega}$ is the measured air weight flow rate and V_j the jet velocity computed according to Eq (1.1). Since the jet momentum coefficient varied slightly for a given run, a nominal jet momentum coefficient, corresponding to the set tunnel Mach number, plenum total pressure, and average plenum total temperature is designated C_μ and is used to identify the data here. The actual C_μ values for each data point are given in Reference 6.

The model was tested with two nozzle configurations (each nozzle configuration corresponds to a given set of 10 orifices on each side being operational). These nozzle configurations were statically calibrated in the tunnel, with all lifting surfaces removed, to obtain six-component force and moment data as a function of plenum pressure. The resulting linear calibration equations were used to correct the aerodynamic data for thrust effects as detailed in Reference 6.

Tests were conducted over a Mach number range of 0.3 to 0.8, which corresponds to a Reynolds number range of 1.5×10^6 to 3.0×10^6 based on the wing mean geometric chord. The angle of attack range was -2° to 30° (reduced to 22° for $M > 0.5$ due to balance load limits). Lateral-directional aerodynamic characteristics were determined from runs at sideslip of +5° and -5°. The angles of attack and sideslip were corrected for deflections of the balance and sting support system due to aerodynamic load.

The angle of attack range was obtained through two separate sting setups; one for the range of -2° to 20° and the other for the range of 10° to 30°. Agreement in the region of overlap between the high α-range data and the low α-range data was excellent, serving as an indication of the accuracy of the measurement of loads at the various test conditions. Extensive comparisons of the basic aerodynamic data for this region of overlap are presented in Reference 6.

Drag measurements for the balance were corrected to a condition of freestream static pressure acting on the base of the model.

RESULTS AND DISCUSSION

Plenum Calibration

The longitudinal positioning of the fluid strake relative to the wing was achieved by utilizing two sets of contiguous nozzles, the 10 located most aft and another set of 10 remaining when 4 nozzles at the aft end and 6 nozzles at the front are sealed. This displaces the location of the fluid strake by 2.54 cm (1.0 in.), or approximately 44% of its length. Figure 2.3 shows the axial force generated by the two nozzle configurations described above (with N1 identifying the aft set of 10 orifices, in keeping with the nomenclature of Reference 6). The dashed line represents a best fit fairing for the LH or RH nozzles open only data. The solid line, drawn with a slope twice that of the dashed line, is seen to represent a good fit for the LH and RH nozzles open data, indicating that the plenum was functioning properly. Excellent agreement between the two configurations is also discernible.

Figure 2.4 shows the weight flow rates for the two nozzle configurations as a function of plenum pressure. Test results for both LH and RH nozzles open are shown, as well as data scaled from LH or RH nozzles open only. The solid line represents maximum theoretical weight flow rate assuming zero total pressure loss. The dashed line represents the weight flow rate corresponding to a 20% total pressure loss. This is the estimate (corresponding to a roughness value $\epsilon = 0.0001$ in. for pipe flow through the orifices of $\ell/d = 14.4$) obtained as part of the pretest analysis.

Using the three components of the thrust generated by the discrete jets on each side, estimates of the orientation of the jet sheet in the body axis system were determined for each of the two nozzle configurations. Results are shown in Figures 2.5 and 2.6, in terms of the angles θ and ϕ which represent an approximation to the deflection and declination angles, respectively, for the fluid strake. Again the deflection angle

exceeded the design value due to asymmetric expansion of the flow at the orifice exit. Asymmetric expansion occurs because the nozzle axes are not normal to the fuselage and results in the declination angle ϕ differing from the design value of zero, as well.

Force Data

The experimental data obtained during the wind tunnel test are presented in both plotted and tabulated form in Reference 6. These data show that implementation of the fluid strake increases $C_{L_{max}}$ as well as the angle of attack at which $C_{L_{max}}$ occurs, and results in an improvement in the drag polars at high C_L.

Data analyses, including comparison with theory, tradeoff considerations for complete configurations and comparisons with another lift-enhancement concept, are presented here.

Lift Augmentation. Four different locations of the fluid strake relative to the wing were tested, corresponding to two nozzle configurations N1, N2 described previously and the two wing locations W1, W2 (mid- and low-wing, respectively).

The decision on optimum location for the fluid strake was made by examining the lift augmentation ratio, $\Delta C_L/C_\mu$, for the four basic configurations tested. The effect of α and C_μ on this parameter is shown in Figures 2.7 and 2.8, at M = 0.3 and 0.7, respectively. With increasing α, the augmentation ratio increases from initial negative values (where lift decrements, similar to the lift loss experienced with low-position physical strakes at low α, occur) to a maximum value at approximately 22°. Configurations W2N1 and W1N1 experience better lift augmentation than W1N2 or W2N2. Configuration W1N1 was judged to be marginally better than configuration W2N1, particularly for the lowest blowing rate, $C_\mu = 0.05$. Unless specifically noted otherwise, all aerodynamic data presented in the rest of this report are based on the optimum configuration, W1N1.

The largest augmentation ratio of 3 was obtained for the lowest value of C_μ. At that blowing rate the implementation of the fluid strake results in three times the lift that could be obtained as a reaction force to directing the thrust of the jet sheet downward and perpendicular to the freestream. The efficiency of the fluid strake decreases with increasing jet momentum coefficient, a trend which has also been noted in investigations of spanwise blowing (Reference 3) and is typical of most jet-augmentation systems.

Figures 2.7 and 2.8 show that the fluid strake becomes more effective than directing the thrust of the jet sheet downward and perpendicular to the freestream, in terms of increasing lift, at angles of attack above 13° to 17° (depending on C_μ and Mach number).

Figure 2.9 shows the lift augmentation ratio for the optimum configuration, W1N1, at M = 0.5. It may be noted that in Figures 2.7(a), (b) and Figure 2.9 implementation of the fluid strake at $C_\mu = 0.05$ results in a lift loss at very high angle of attack. This is probably the result of loss of body-generated lift, in an angle of attack range where the low-momentum jet sheet does not generate a strong enough vortex to keep the wing from stalling.

The lift augmentation ratio for the configuration with horizontal tail added (W1N1H) is shown in Figure 2.10. By comparing it with Figures 2.7(a) and 2.8(a) it can be seen that adding the horizontal tail reduces the effectiveness of the fluid strake at the higher angles of attack. The same observation has been reported by investigators of the spanwise blowing concept (Reference 5). Data presented later in this report will show that this reduction is due to a decrease in the lift contribution of the horizontal tail itself.

The effect of C_μ and Mach number on the lift augmentation ratio at a fixed angle of attack is summarized in Figures 2.11 and 2.12. The lift augmentation ratio generally decreases with increasing C_μ and is seen to be essentially constant with Mach number for the range tested.

Lift Effectiveness. The percentage increase in lift generated by the fluid strake is presented in Figure 2.13, where the parameter $C_L/C_{L,o}$ is the lift with blowing on (but corrected for thrust effects) divided by the lift for the unblown configuration. For a given C_μ, $C_L/C_{L,o}$ increases with α until a maximum occurs at $\alpha \approx 22°$.

The experimental results are compared with theoretical predictions which assume a stable, fully developed leading-edge vortex flow. The leading-edge suction analogy (References 8, 9) was used to calculate $C_{L,tot}/C_{L,p}$, which is the ratio of full vortex flow lift to attached potential flow lift. It should be noted that the theory does not account for the effect of C_μ but represents the full vortex-induced lift increments, assuming a fully developed vortex with no vortex breakdown. The lift data for the highest C_μ value agree fairly well with the full-vortex lift estimates and indicate that with increased C_μ the full-vortex lift estimates can be exceeded. Considering that in a design

application limits on the level of C_μ must be imposed, the lift levels predicted by the leading-edge suction analogy do represent design guidelines on the maximum lift that can be achieved.

Horizontal Tail Performance. The effect of the fluid strake on the lift contribution of the horizontal tail is shown in Figure 2.14. At M =0.3 increasing C_μ increases the lift contribution of the horizontal tail up to $\alpha \approx 14°$; at angle of attack larger than 14°, the lift contribution of the horizontal tail decreases with increased C_μ, as the fluid strake increases the lift on the wing with consequent increased downwash over the horizontal tail resulting in a reduced effective angle of attack for the horizontal tail. The same trends are discernible at M = 0.7.

Vertical Tail Effectiveness. Figure 2.15 shows the influence of the fluid strake on vertical tail effectiveness at M = 0.3, 0.5. Increasing C_μ leads to a small improvement in vertical tail effectiveness between 15° and 28° angle of attack, and delays the loss of directional stability to a higher angle of attack.

Effective dihedral due to the vertical tail is shown in Figure 2.16. Figure 2.16 shows that the influence of the fluid strake on effective dihedral is small in the region of α where the parameter indicates a stable behavior for the configuration with $C_\mu = 0$.

Effect on Maneuver Performance

Although the fluid strake concept improves aerodynamic characteristics significantly, its impact on total aircraft performance must be evaluated by accounting for reduction of main-engine thrust. An attempt to demonstrate the effects of implementing the fluid strake on aircraft performance is made here.

For demonstration purposes, engine thrust, weight and wing loading have been assumed, based on typical T/W ratios for fighter aircraft. The aerodynamic terms are scaled from data for W1N1 at the corresponding Mach numbers. The lift and drag forces used are the total loads for the configuration and, thus, include the thrust components from the jet sheet which are recovered as vectored lift or as thrust.

The standard engine thrust is reduced by $C_\mu qS$ when the fluid strake is implemented. This estimate does not account for losses associated with generating the required blowing either through engine bleed or through an auxiliary propulsion system. The impact of weight penalties associated with a fluid strake system is also not reflected,

as such an evaluation is considered to be beyond the scope of this study.

Specific excess power available for maneuvering as a function of load factor is presented in Figures 2.17, 2.19, 2.21 for operation at three different altitudes and Mach numbers. The assumed variation of thrust with altitude simulates typical fighter aircraft engine characteristics.

The effective L/D for the configuration, at the same operating conditions and subject to the same assumptions, has been plotted vs C_L in Figures 2.18, 2.20 and 2.22. The ratio accounts for the contribution of main-engine thrust to lift and its effective contribution to the drag term when operating at angle of attack. It also takes into account the reduction in engine thrust and resulting effective drag penalty due to the thrust diverted to generate the jet sheet.

The results show that the fluid strake increases the specific excess power available at the higher load factors and allows higher load factors to be attained. At Mach numbers of 0.5 and 0.7 this payoff in specific excess power is realized at load factors higher than those which can be sustained. Similarly, a payoff in effective L/D is realized at lift coefficients higher than approximately 0.8.

Aerodynamic data from an investigation of the spanwise blowing concept (Ref 10) have been utilized in combination with the previously stated assumptions on engine thrust and aircraft weight to generate Figures 2.23 and 2.24. It should be noted that the aerodynamic data of Reference 10 are for a configuration which differs from the one employed in this study, so that data at $C_\mu = 0$ cannot be compared. Improvements in performance over the unblown configuration show a marked similarity to the gains derived from the fluid strake, for corresponding values of the jet momentum coefficient.

CONCLUSIONS

The concept of lift enhancement at high angle of attack using a jet sheet formed by blowing through a series of small in-line orifices in the side of the fuselage ahead of the wing was tested on a general research fighter model over a range of Mach numbers and jet momentum coefficients. Effects on horizontal and vertical control surfaces were determined. The impact of the concept on overall aircraft performance was evaluated by integrating it into an assumed aircraft design. The following conclusions were formed:

- The favorable vortex flow induced by the jet sheet results in significant improvements in the aerodynamic characteristics; $C_{L_{max}}$ is improved, the angle of attack at which $C_{L_{max}}$ occurs is increased and improved drag polars at high C_L result.
- Lift augmentation ratios show that the fluid strake becomes more lift-effective than directing its thrust downward and perpendicular to the freestream at angles of attack of 13° to 17°. The effectiveness of the fluid strake decreases with increasing C_μ and was essentially constant with Mach number.
- The vortex flow induced by the jet sheet increased the vertical tail effectiveness and delayed loss of directional stability to higher angle of attack.
- Taking into account thrust losses equal to $C_\mu qS$ due to the blowing requirements of the fluid strake, specific excess power and effective L/D are improved at high lift coefficients and are comparable to gains achieved by spanwise blowing. However, these results are for a wing without variable camber and are untrimmed. The effects of the fluid strake in the presence of flap deflections typical of maneuvering conditions need to be determined.
- The fluid strake concept, by generating additional lift at moderate angle of attack, might have utility as an aid to either short takeoff or low-speed maneuvering. In either case, for a fixed amount of air available, much higher jet momentum coefficients are achieved than for high-speed maneuvering.

REFERENCES

1. Wentz, William H., Jr.; and Kohlmann, David L.: Wind Tunnel Investigations of Vortex Breakdown on Slender Sharp-Edged Wings. NASA CR-98737, 1968.

2. Henderson, William P.; and Huffman, Jarrett K.: Effect of Wing Design on the Longitudinal Aerodynamic Characteristics of a Wing-Body Model at Subsonic Speeds. NASA TN D-7099, 1972.

3. Campbell, James F.: Augmentation of Vortex Lift by Spanwise Blowing. AIAA Paper No. 75-993, August 1975.

4. Erickson, Gary E.; and Campbell, James F.: Augmentation of Maneuver Performance by Spanwise Blowing. NASA TM X-73998, 1977.

5. Erickson, Gary E.; and Campbell, James F.: Improvement of Maneuver Aerodynamics by Spanwise Blowing. NASA TP-1065, 1977.

6. Huffman, Jarrett K.; Fox, Charles H., Jr.; and Ziegler, Henry: Subsonic Longitudinal and Lateral-Directional Static Aerodynamic Characteristics of a General Research Fighter Configuration Employing a Jet Sheet Vortex Generator. NASA TM 74049, 1978.

7. Knystautas, R.: The Turbulent Jet from a Series of Holes in Line. The Aeronautical Quarterly, Vol. XV, February 1964, pp. 1-28.

8. Polhamus, Edward C.: Predictions of Vortex Lift Characteristics by a Leading-Edge Suction Analogy. J. Aircraft, Vol. 8, No. 4, April 1971, pp. 193-199.

9. Lamar, John E.; and Gloss, Blair B.: Subsonic Aerodynamic Characteristics of Interacting Lifting Surfaces with Separated Flow Around Sharp Edges Predicted by a Vortex-Lattice Method. NASA TN D-7921, 1975.

10. Bradley, R.G.; Wray, W.O.; and Smith, C.W.: An Experimental Investigation of Leading-Edge Vortex Augmentation by Blowing. NASA CR-132415, 1974.

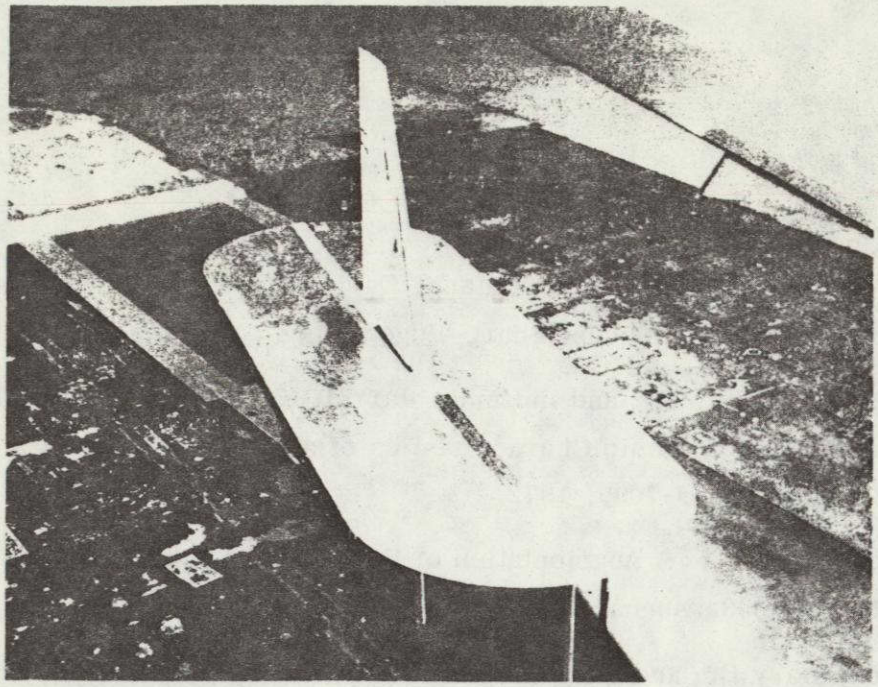

(a) Wing and Splitter Plate

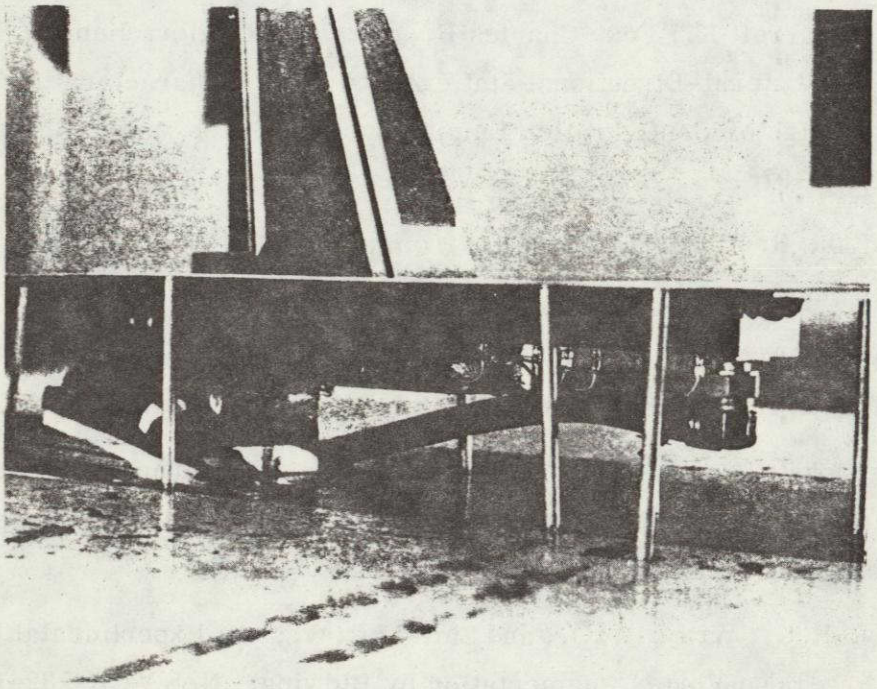

(b) Details of Plenum and Balance beneath Splitter Plate

FIGURE 1.1. HALF-SPAN MODEL INSTALLATION

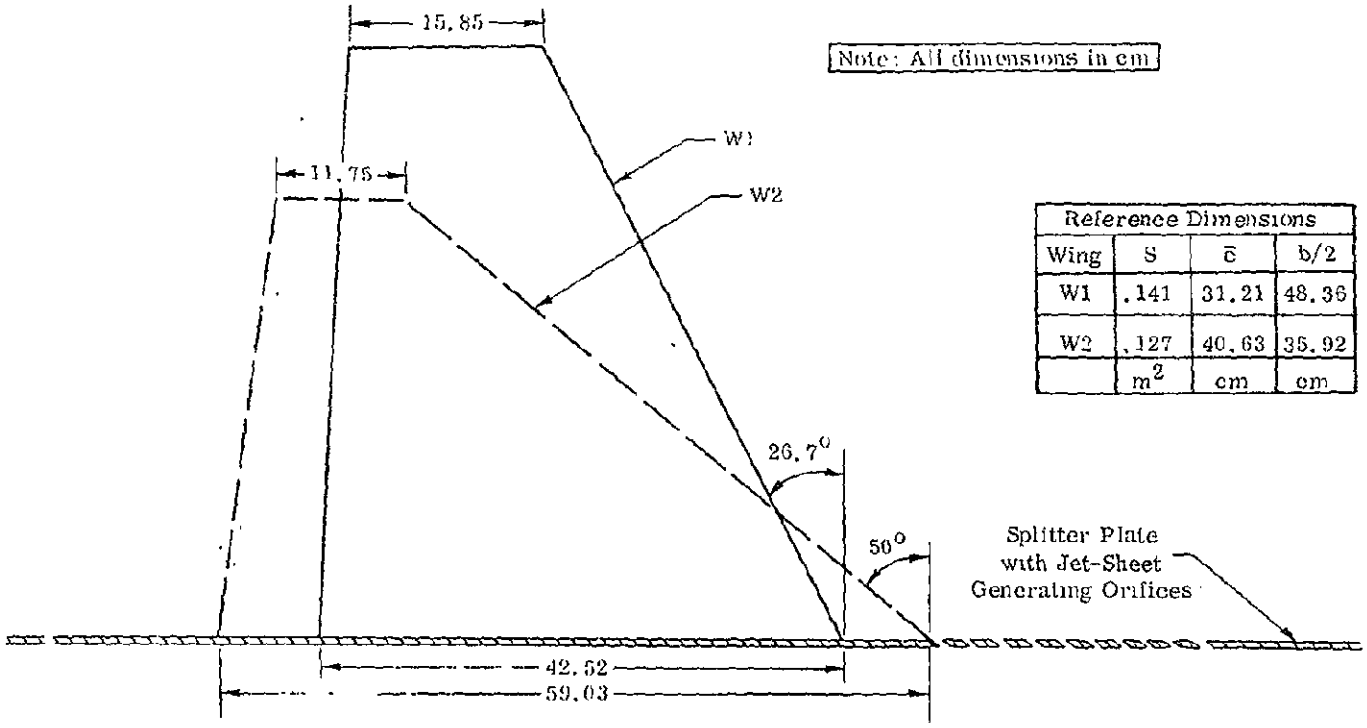

Reference Dimensions			
Wing	S	$\bar{c}$	b/2
W1	.141	31.21	48.36
W2	.127	40.63	35.92
	m^2	cm	cm

FIGURE 1.2. GEOMETRY OF WINGS TESTED

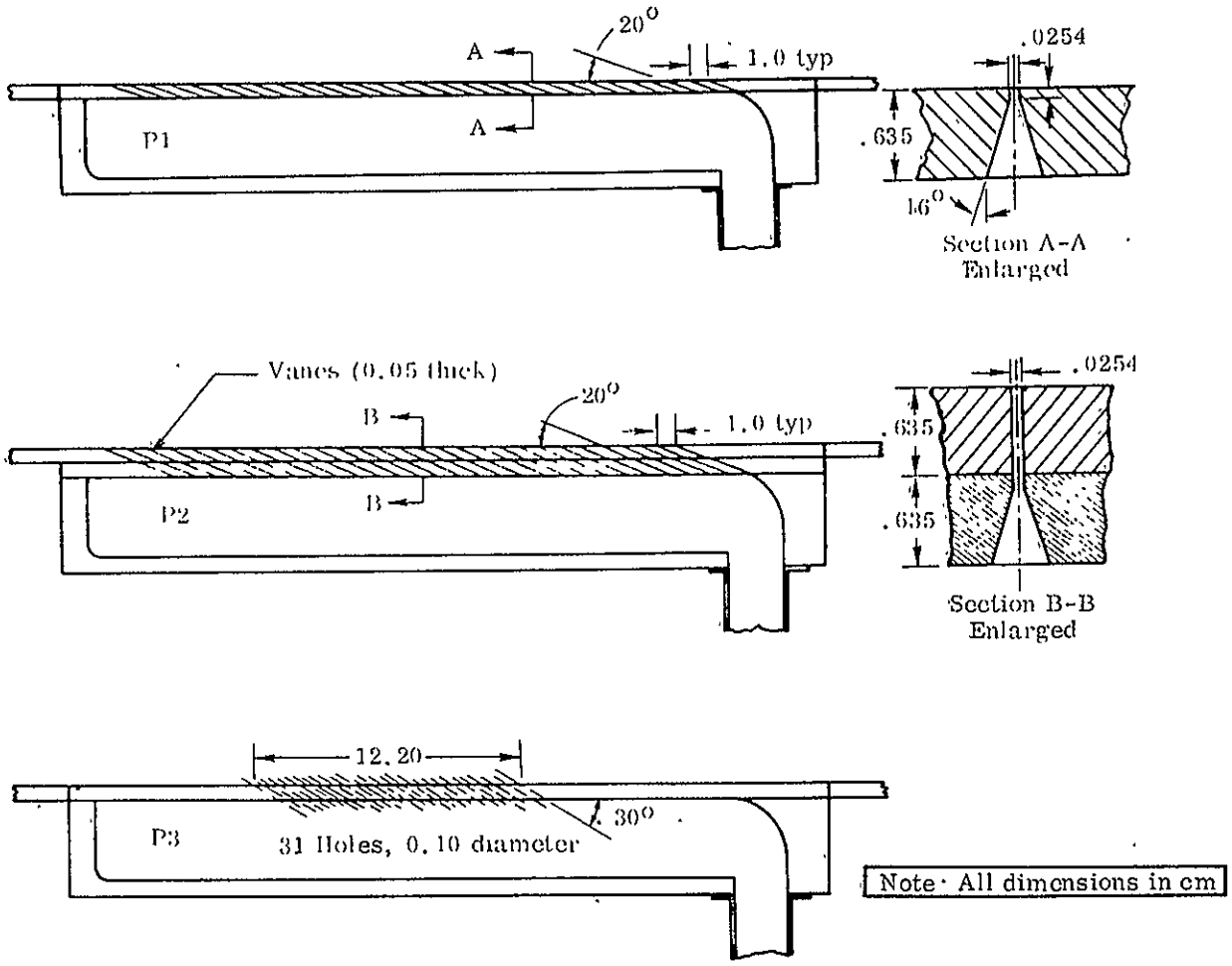

FIGURE 1.3. DETAILS OF PLENUM-COVER PLATE CONFIGURATIONS

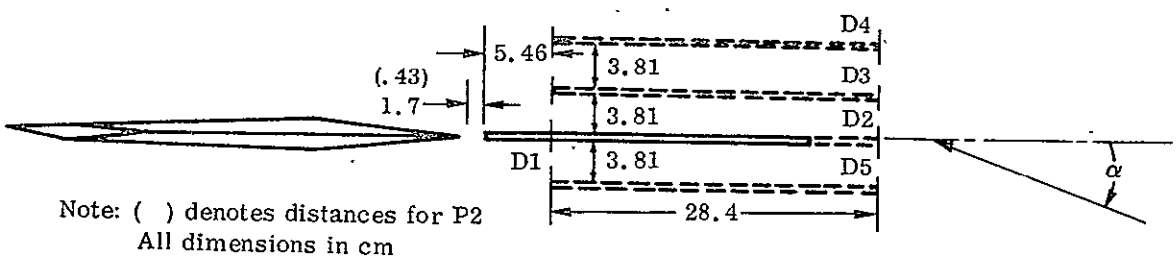

(a) P1, P2 Relative to W1

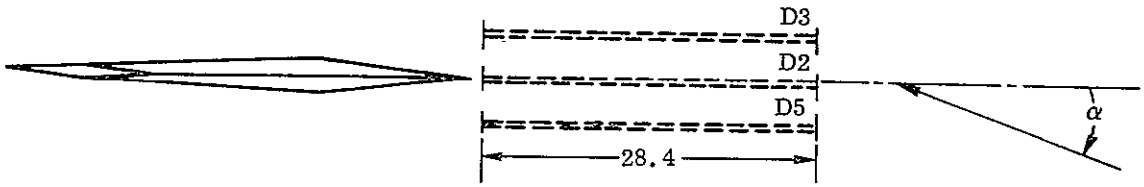

(b) P1, P2 Relative to W2

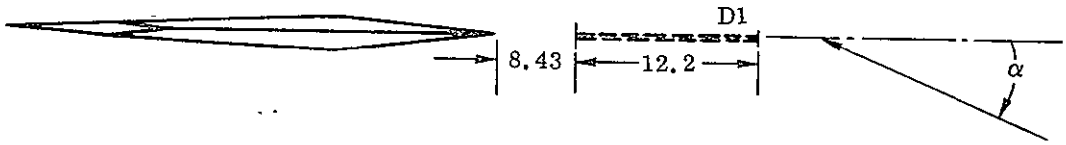

(c) P3 Relative to W1

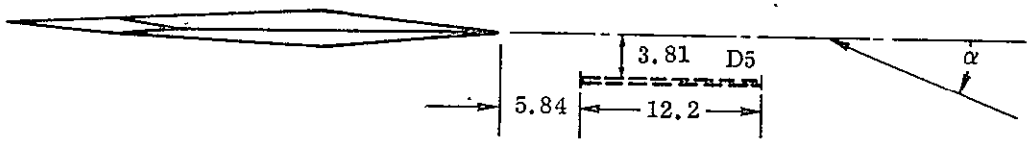

(d) P3 Relative to W2

FIGURE 1.4. LOCATIONS OF FLUID STRAKE RELATIVE TO WING

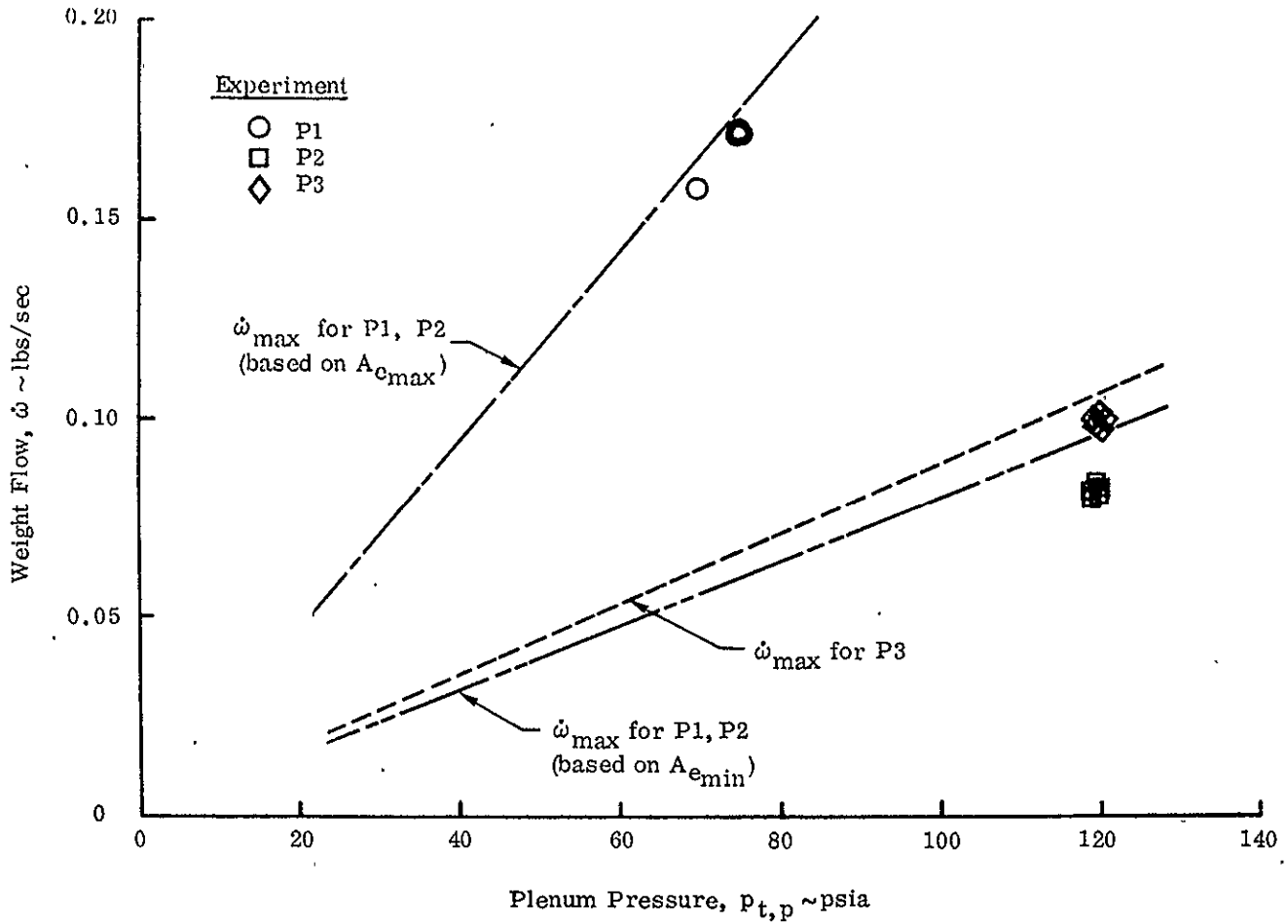

FIGURE 1.5. WEIGHT FLOW RATES

(a) Blowing off: W1, α = 20°, q = 50 psf

(b) Blowing on: W1P1D1, α = 20°, q = 25 psf, $C_\mu \approx 0.09$

FIGURE 1.6. FLOW VISUALIZATION PHOTOGRAPHS

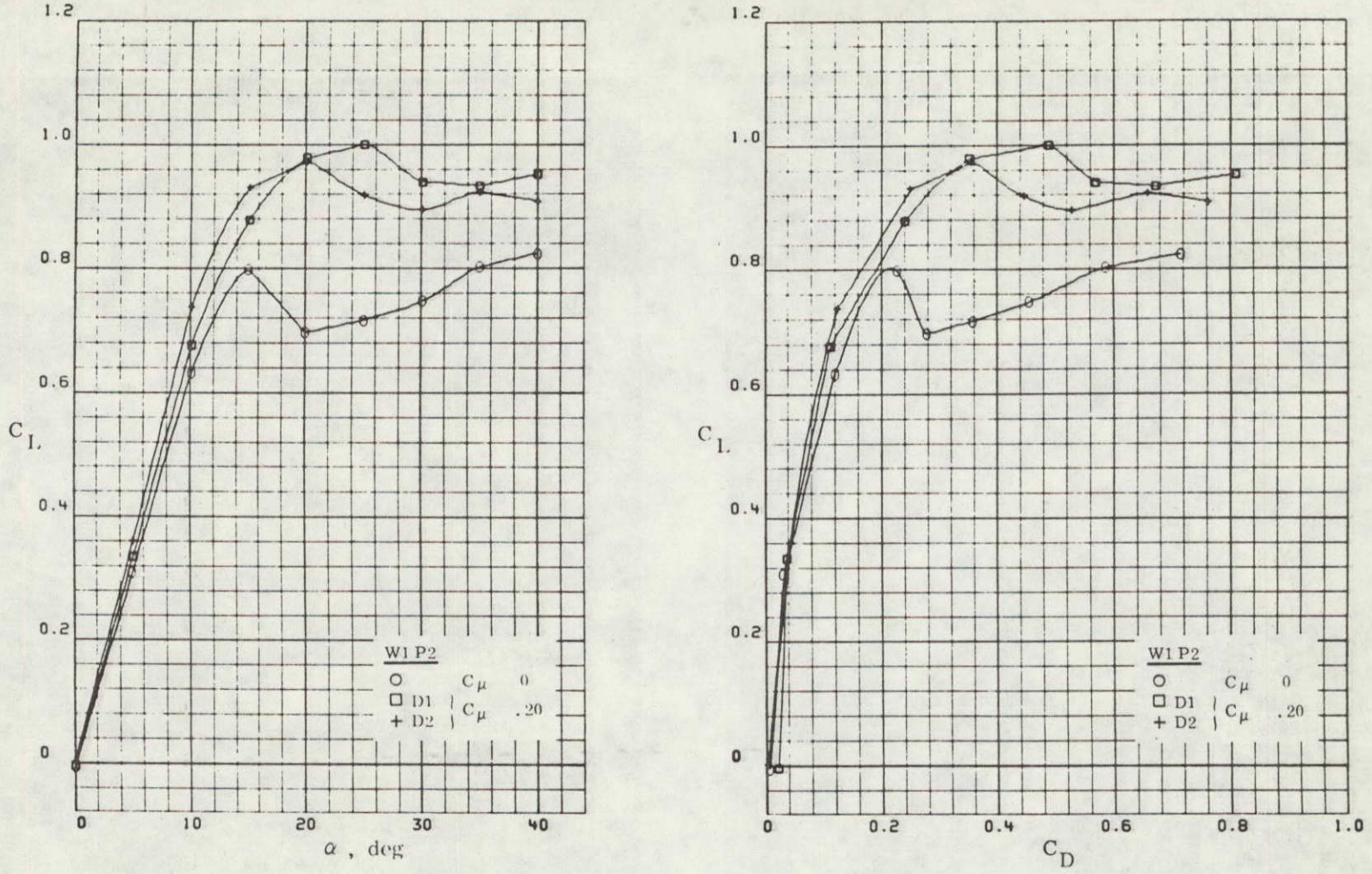

FIGURE 1.7. EFFECT OF HORIZONTAL DISPLACEMENT OF FLUID STRAKE ON AERODYNAMIC CHARACTERISTICS OF WING

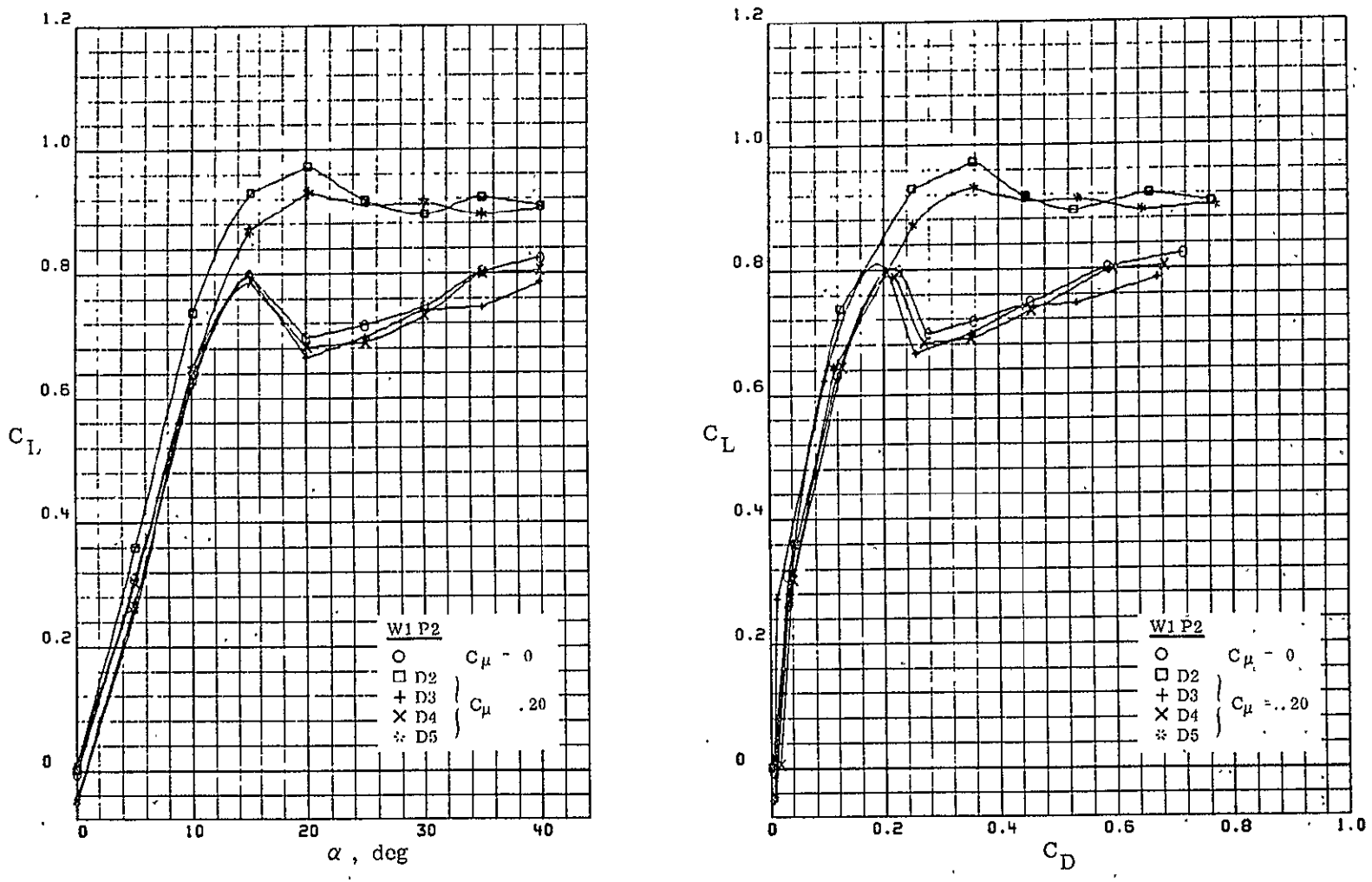

FIGURE 1.8. EFFECT OF VERTICAL DISPLACEMENT OF FLUID STRAKE ON AERODYNAMIC CHARACTERISTICS OF WING

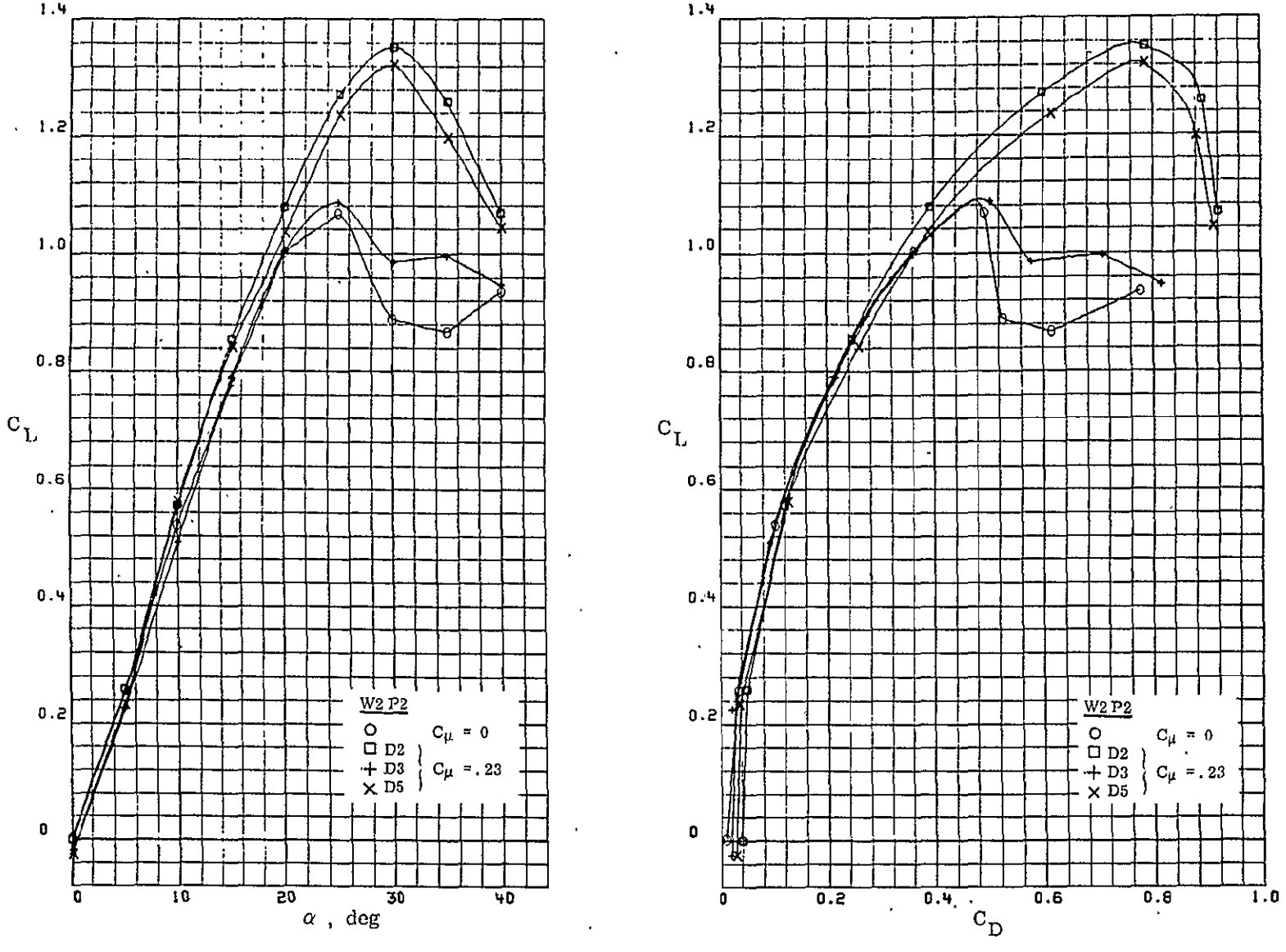

FIGURE 1.9. EFFECT OF VERTICAL DISPLACEMENT OF FLUID STRAKE ON AERODYNAMIC CHARACTERISTICS OF WING

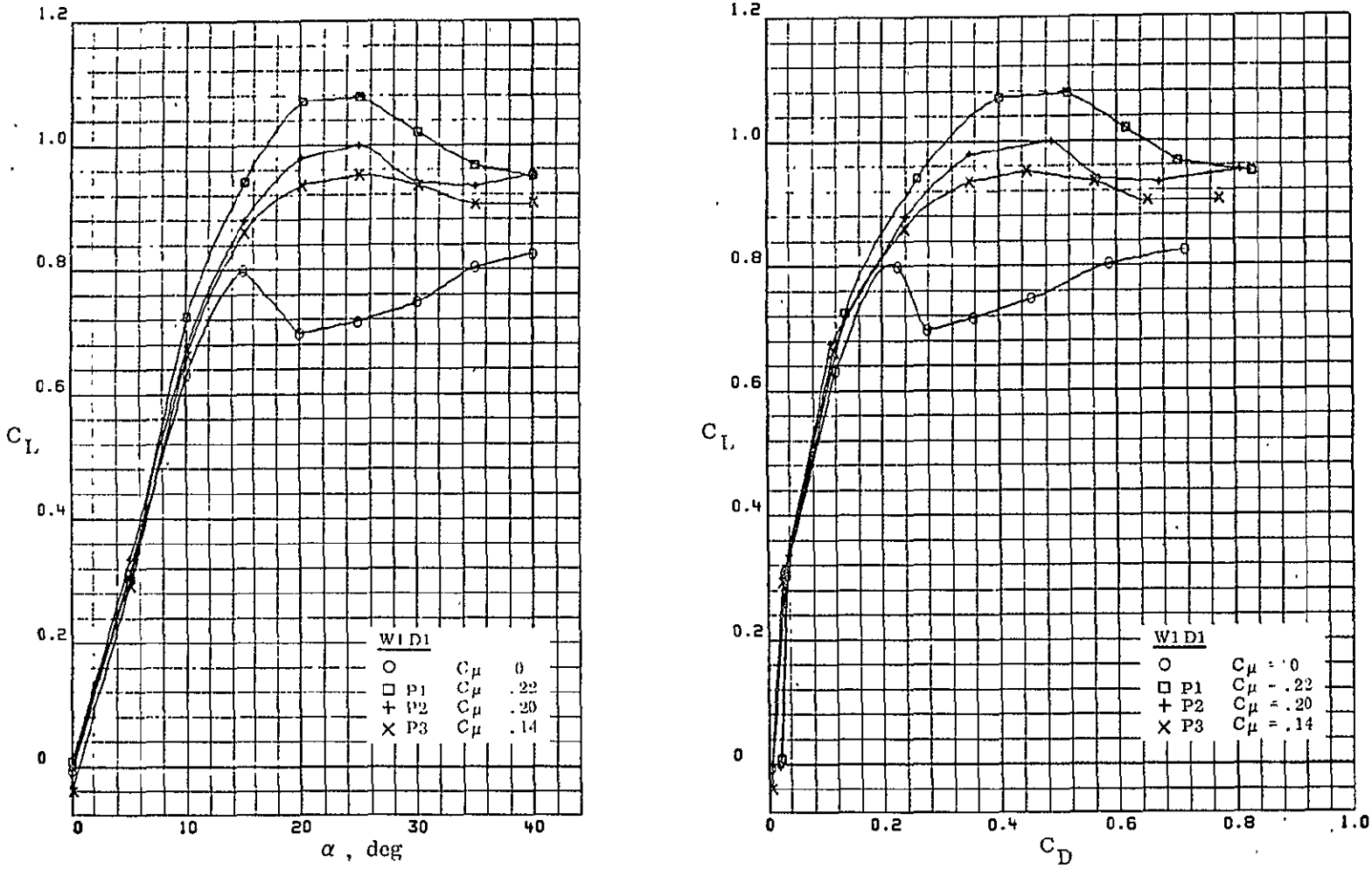

FIGURE 1.10. EFFECT OF ORIFICE SHAPE ON PERFORMANCE OF FLUID STRAKE

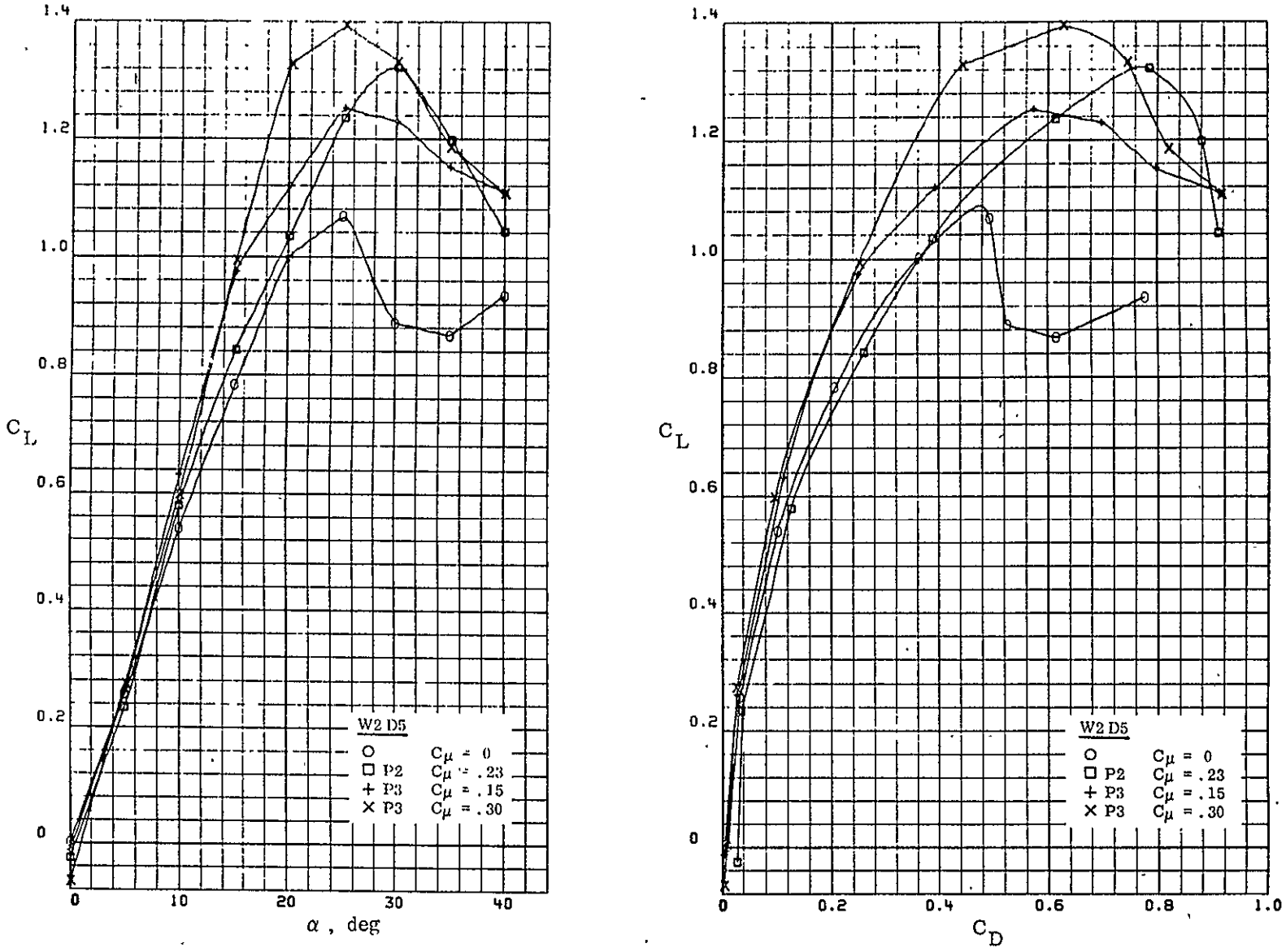

FIGURE 1.11. EFFECT OF ORIFICE SHAPE ON PERFORMANCE OF FLUID STRAKE

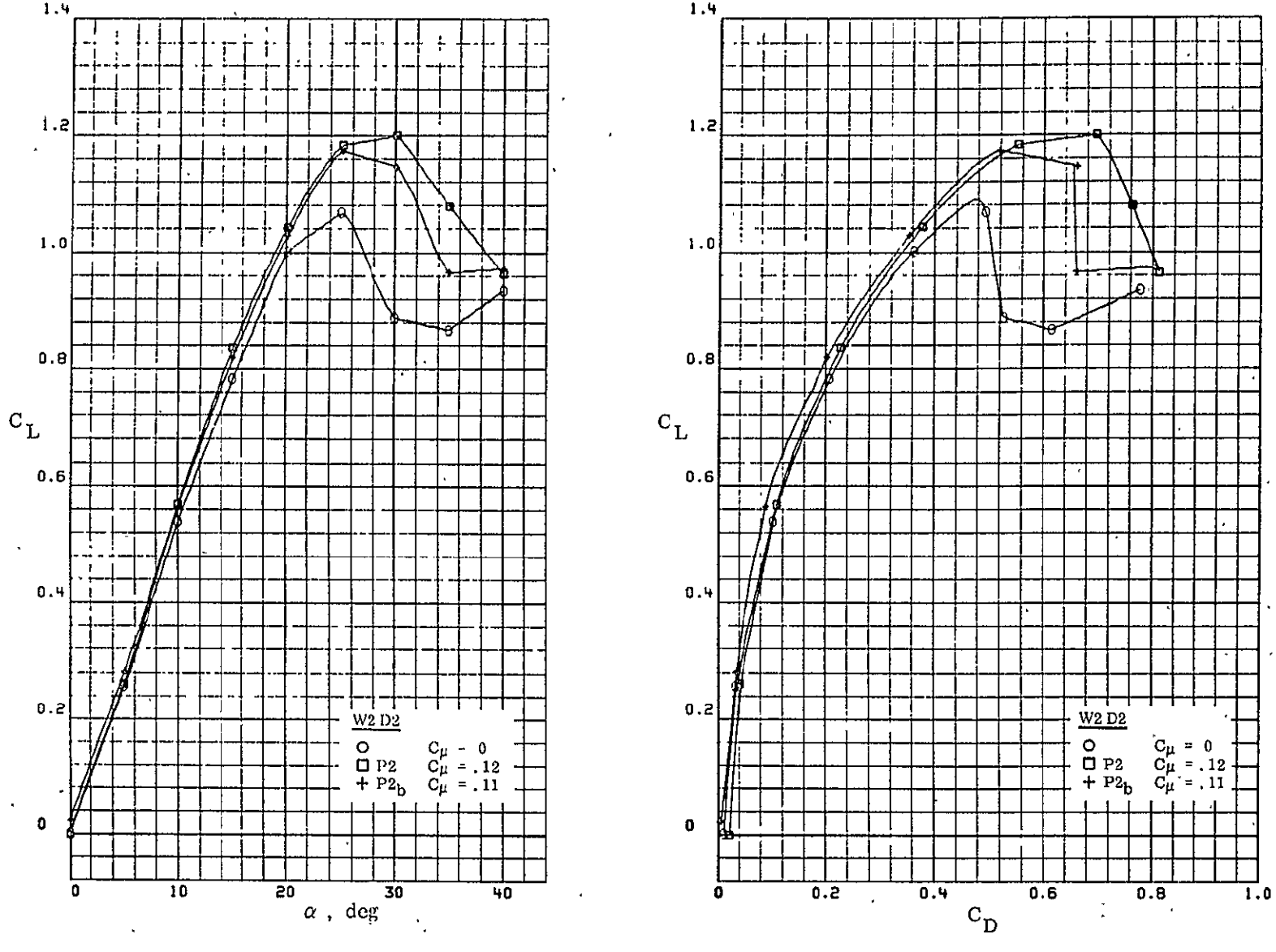

FIGURE 1.12. EFFECT OF JET SHEET CONCENTRATION ON PERFORMANCE OF FLUID STRAKE

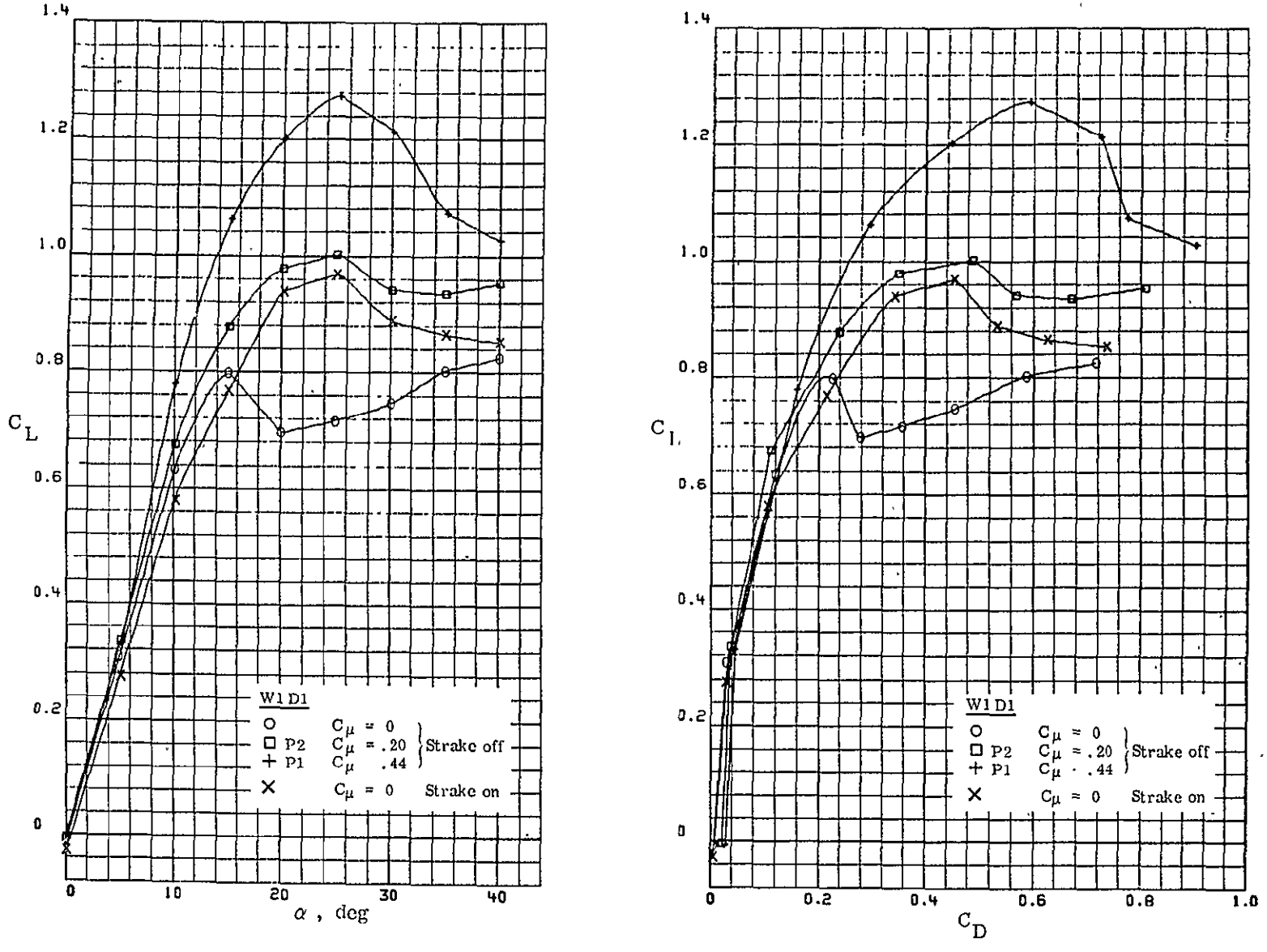

FIGURE 1.13. COMPARISON OF FLUID STRAKE WITH PHYSICAL STRAKE

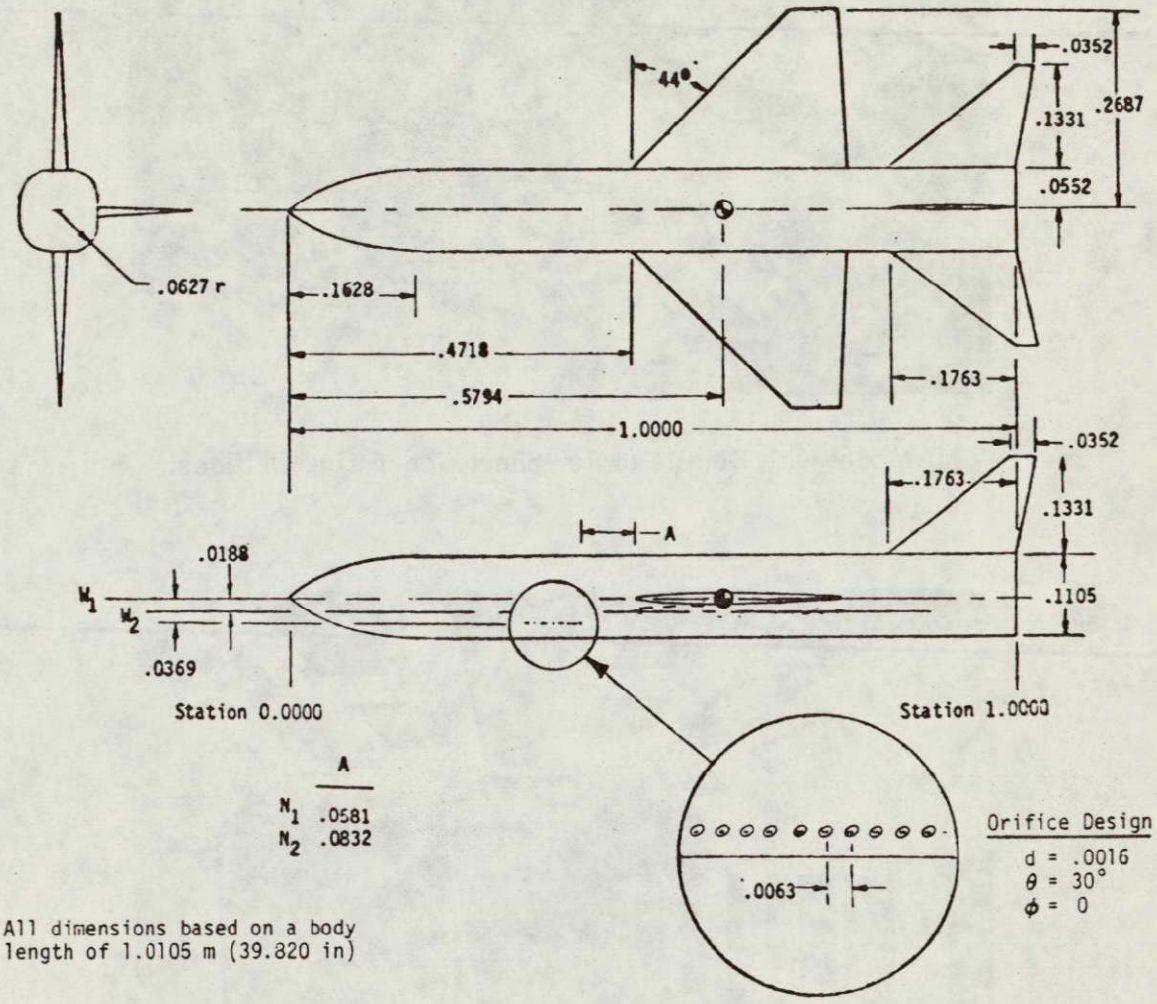

FIGURE 2.1. GEOMETRY DETAILS OF GENERAL RESEARCH MODEL

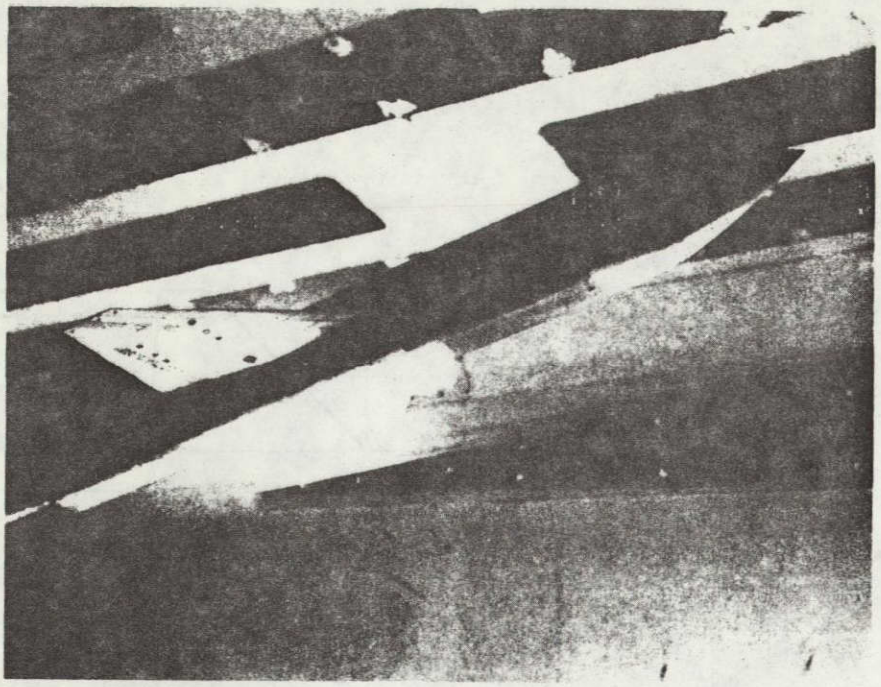

(a) Model with Details of Jet-Sheet Generating Orifices

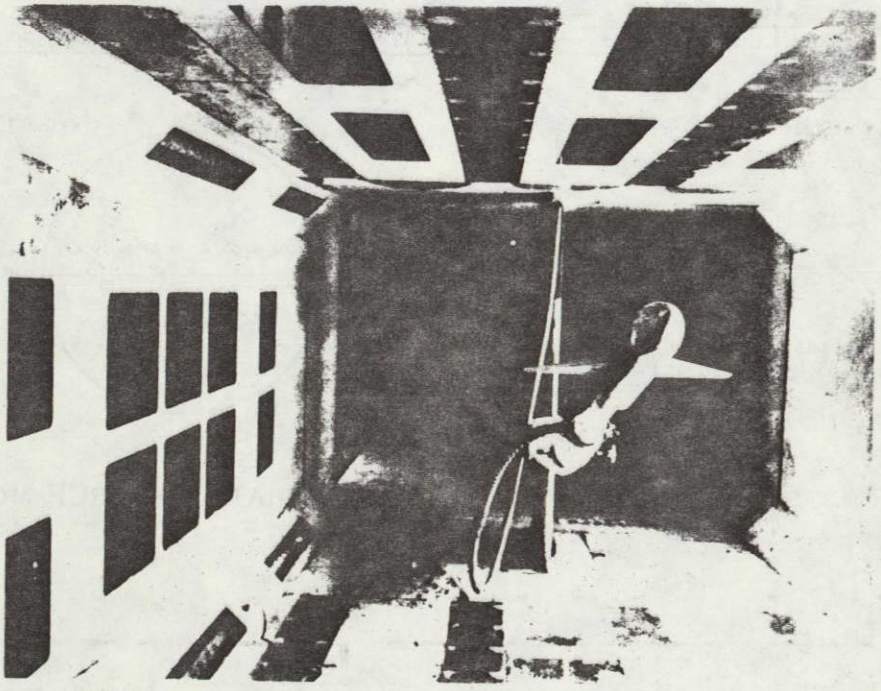

(b) Model with Air Supply Line

FIGURE 2.2. GENERAL RESEARCH MODEL INSTALLATION

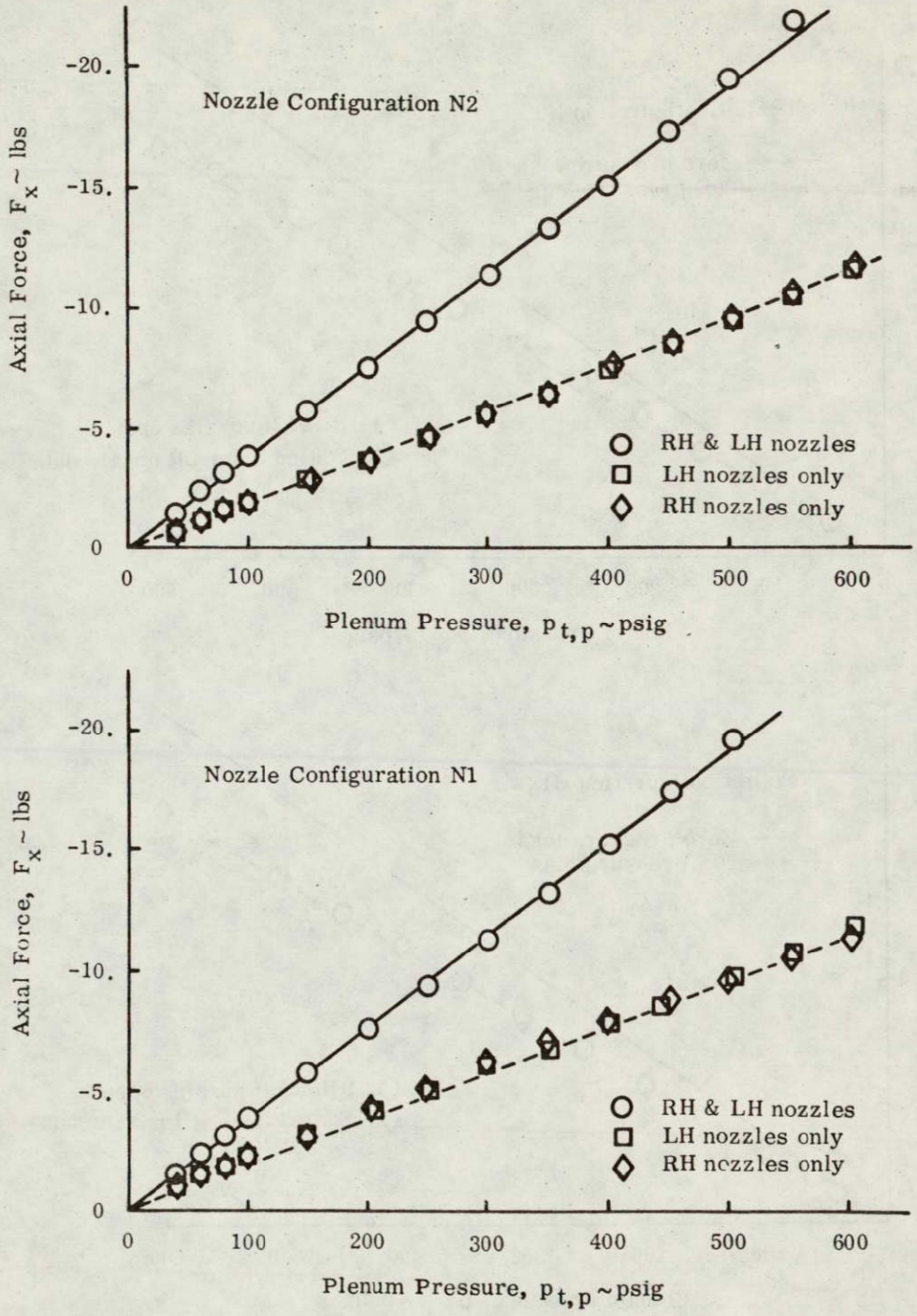

FIGURE 2.3. VARIATION OF AXIAL FORCE WITH PLENUM PRESSURE

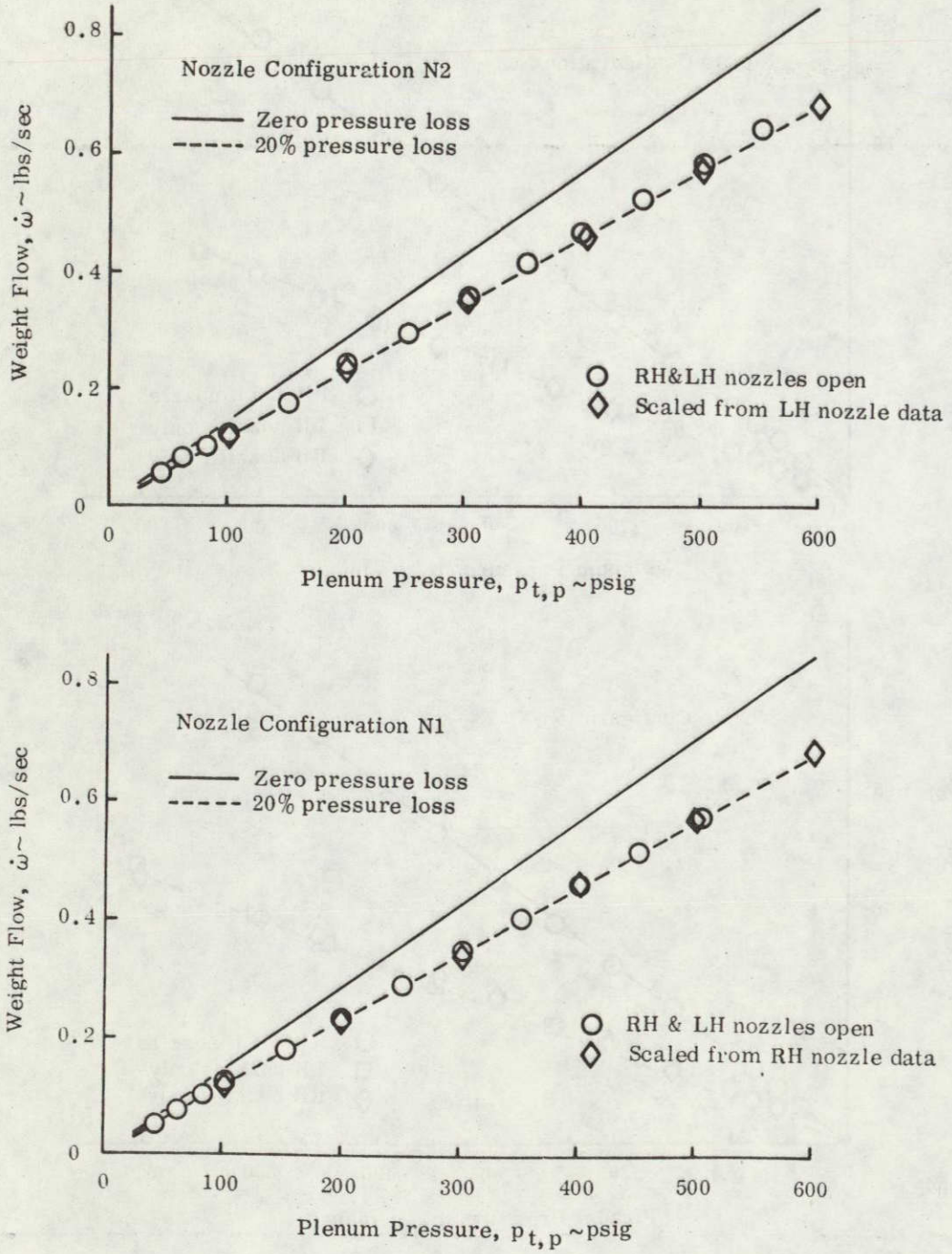

FIGURE 2.4. VARIATION OF WEIGHT FLOW WITH PLENUM PRESSURE

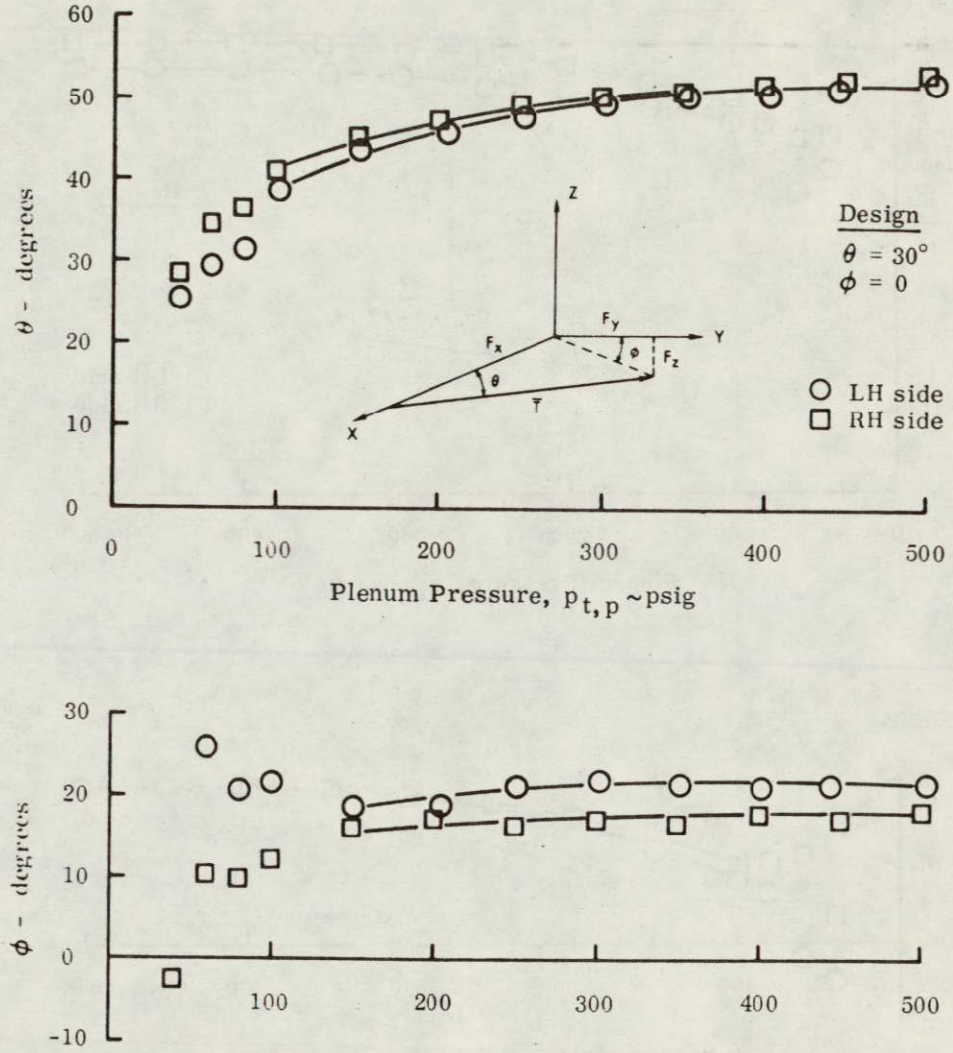

FIGURE 2.5. ORIENTATION OF FLUID STRAKE FOR NOZZLE CONFIGURATION N1

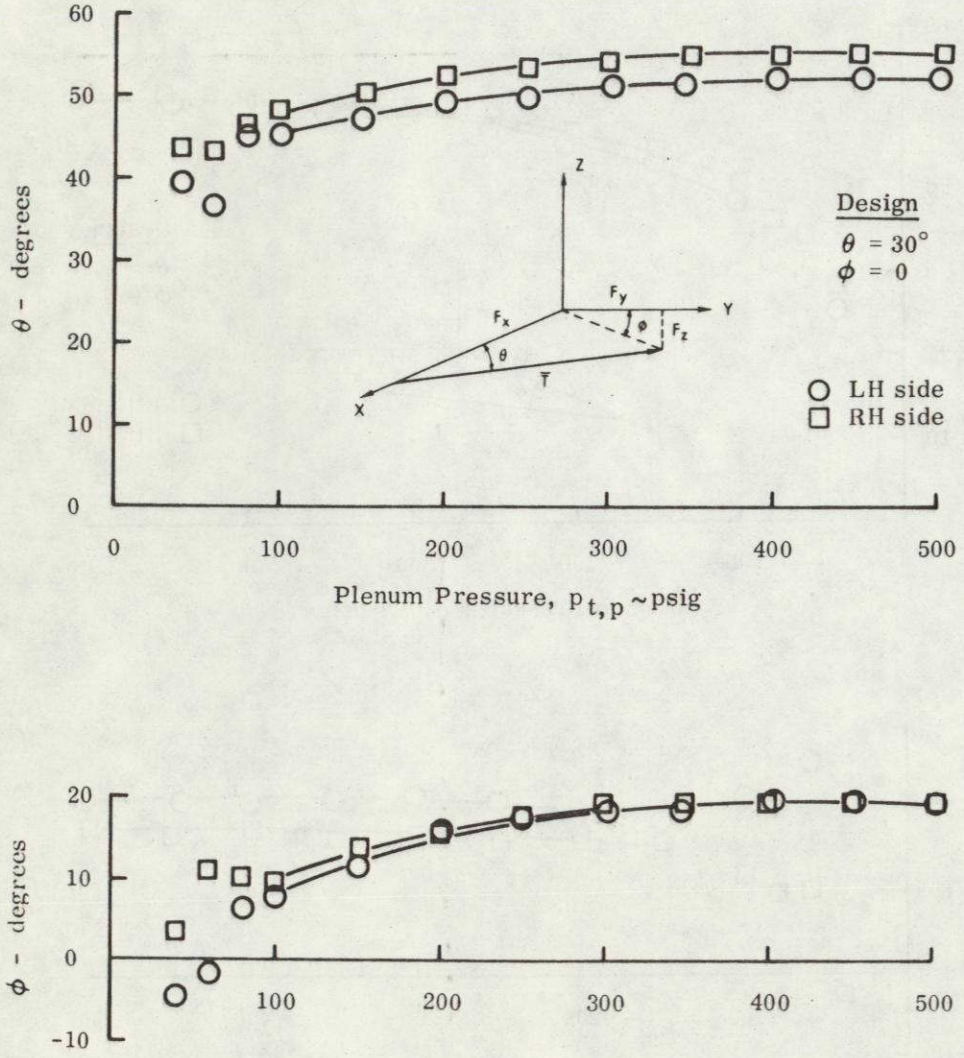

FIGURE 2.6. ORIENTATION OF FLUID STRAKE FOR NOZZLE CONFIGURATION N2

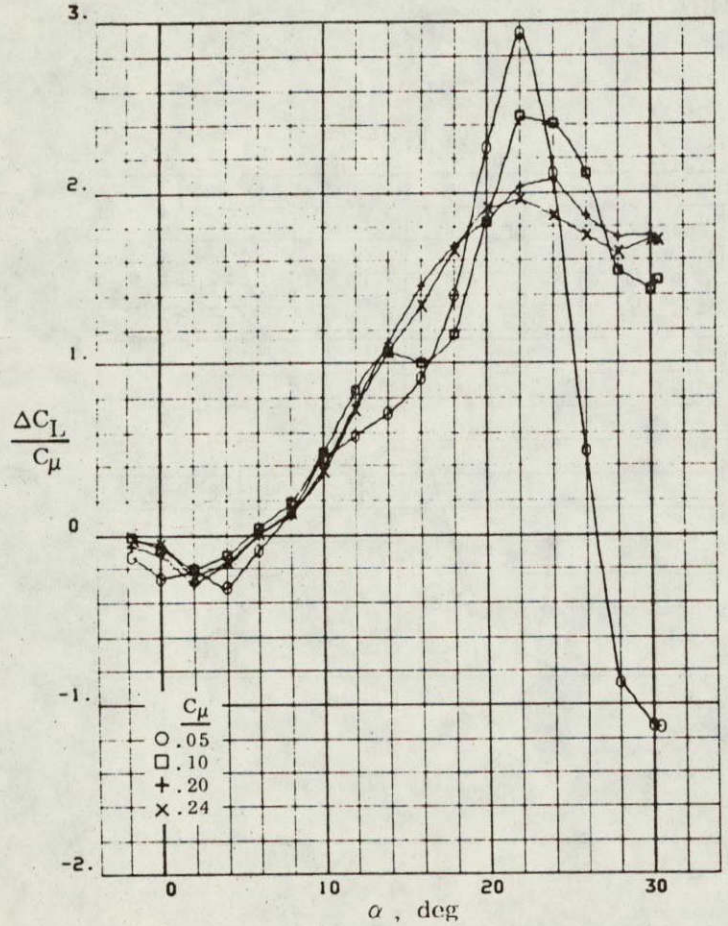

(a) W1N1

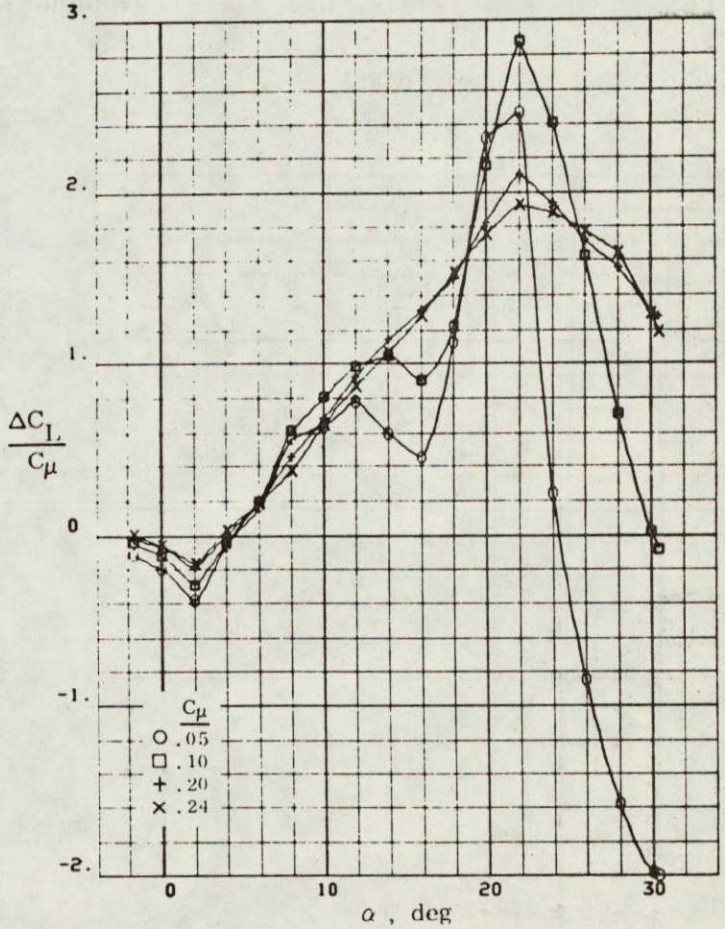

(b) W2N1

FIGURE 2.7. EFFECT OF α AND C_μ ON LIFT AUGMENTATION RATIO (M = 0.3)

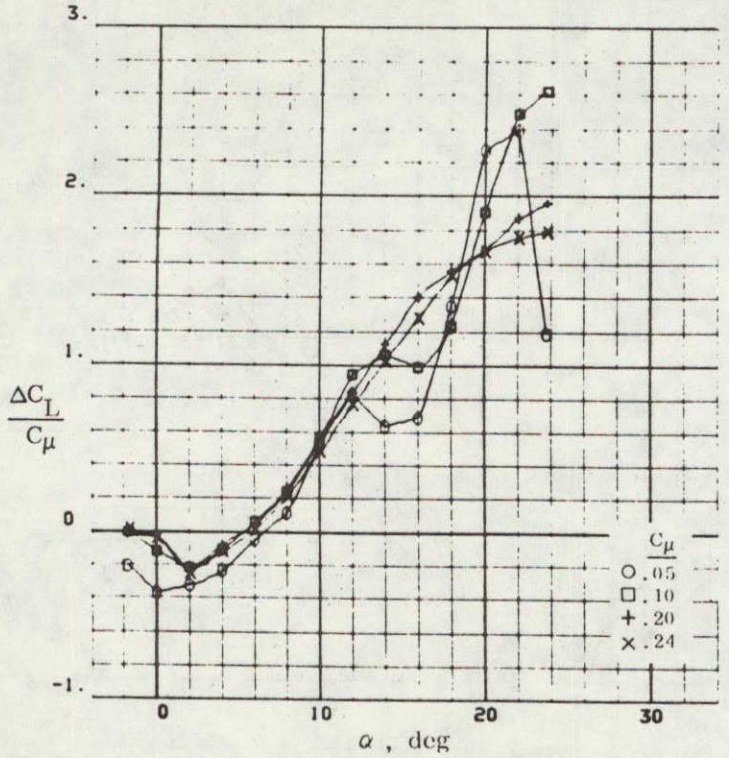

(c) W1N2

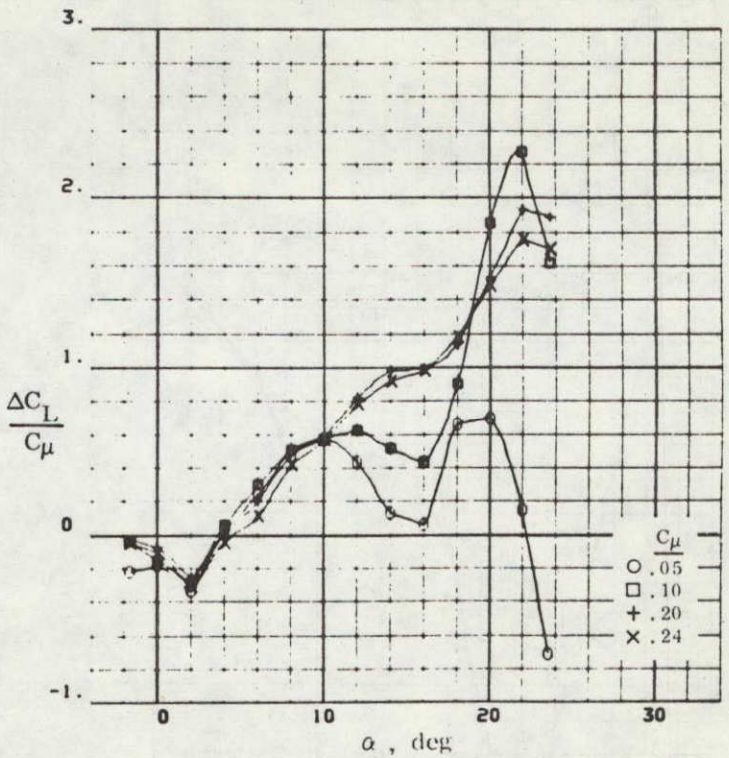

(d) W2N2

FIGURE 2.7. (Concluded)

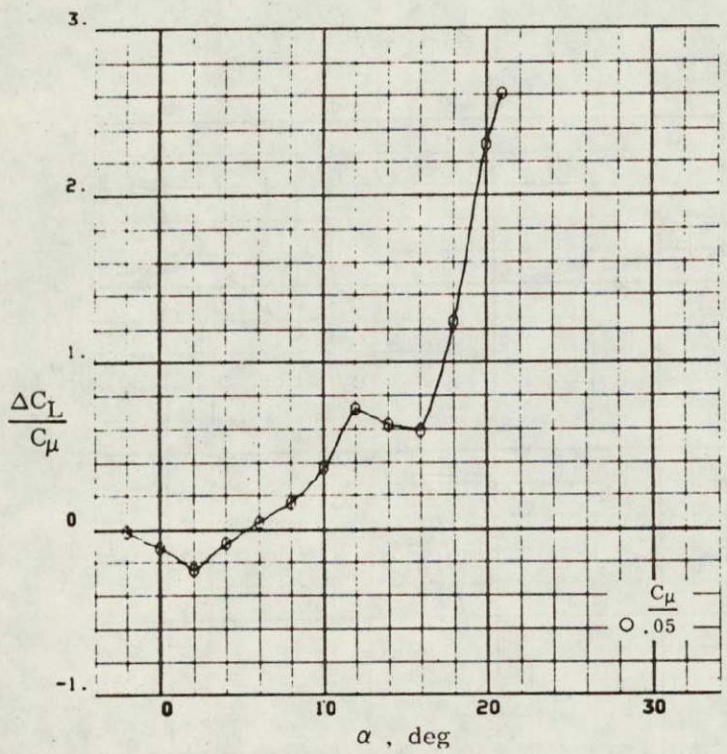

(a) W1N1

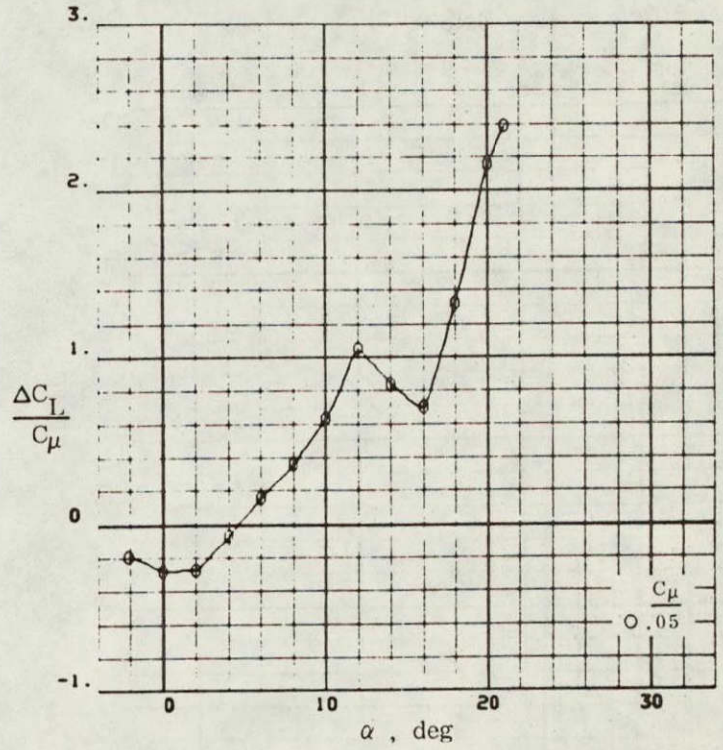

(b) W2N1

FIGURE 2.8. EFFECT OF α AND C_μ ON LIFT AUGMENTATION RATIO (M = 0.7)

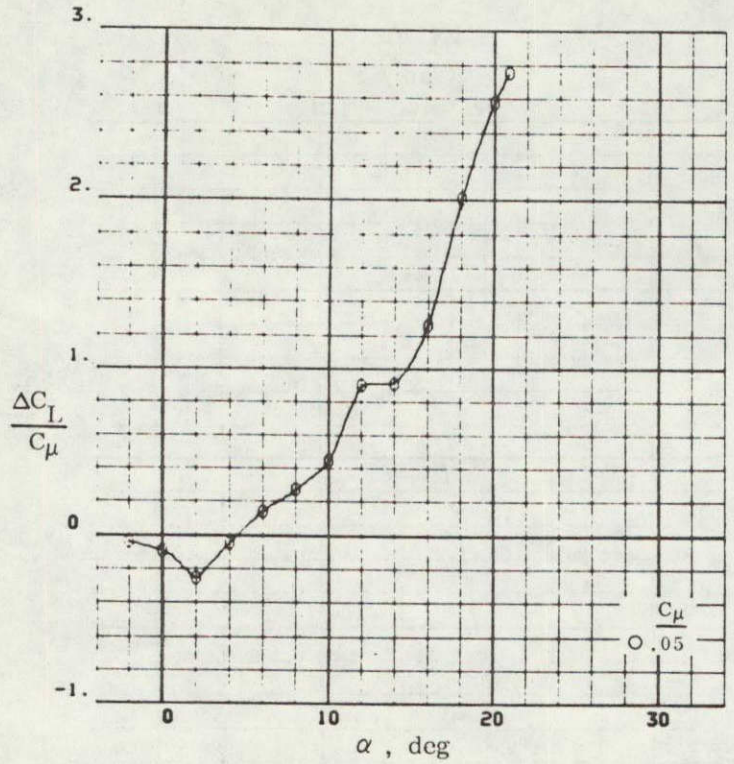

(c) W1N2

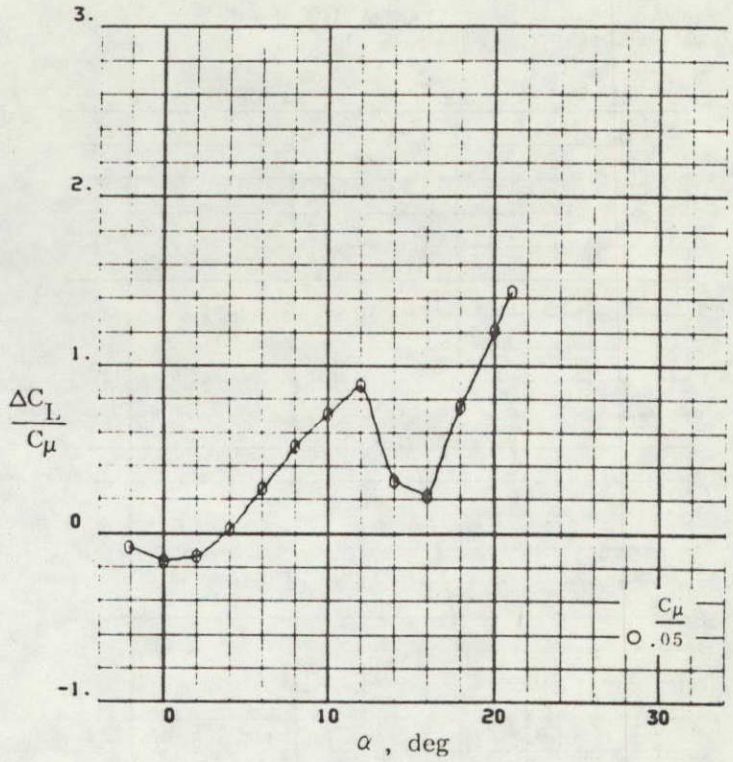

(d) W2N2

FIGURE 2.8. (Concluded)

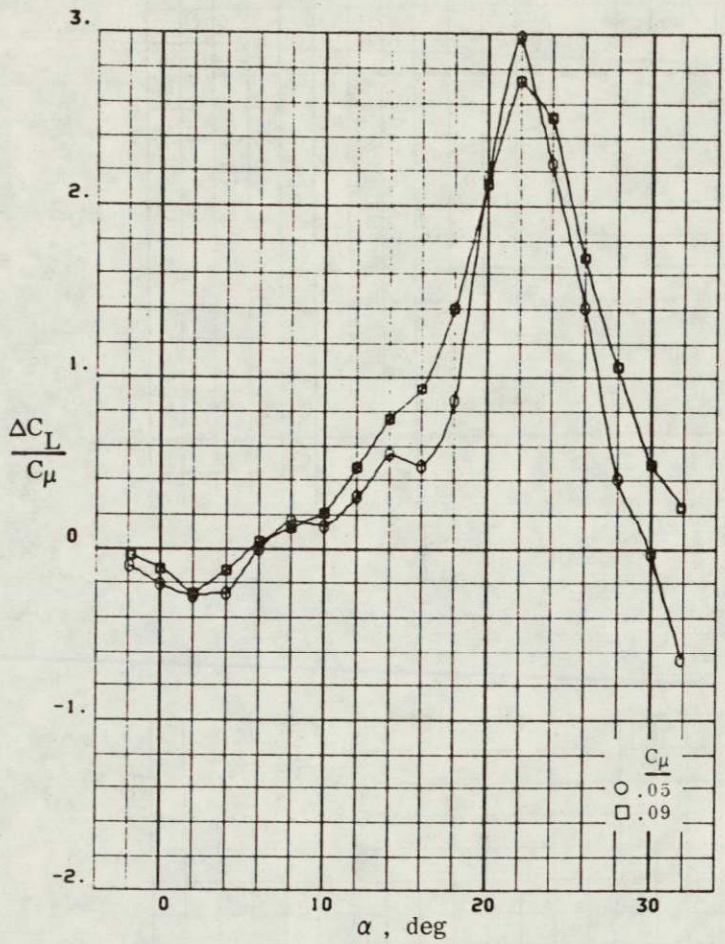

FIGURE 2.9. EFFECT OF α AND C_μ ON LIFT AUGMENTATION RATIO OF OPTIMUM CONFIGURATION (W1N1) AT M = 0.5

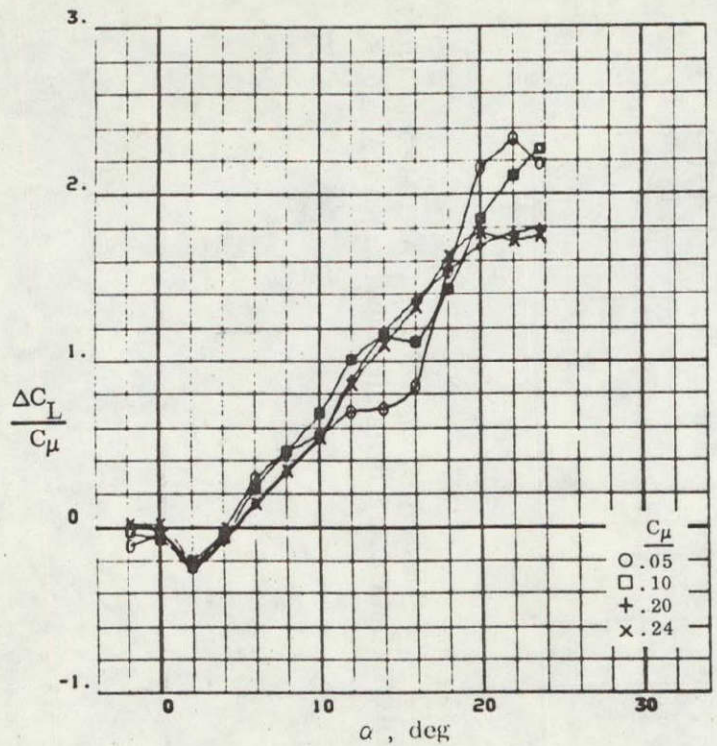

(a) M = 0.3

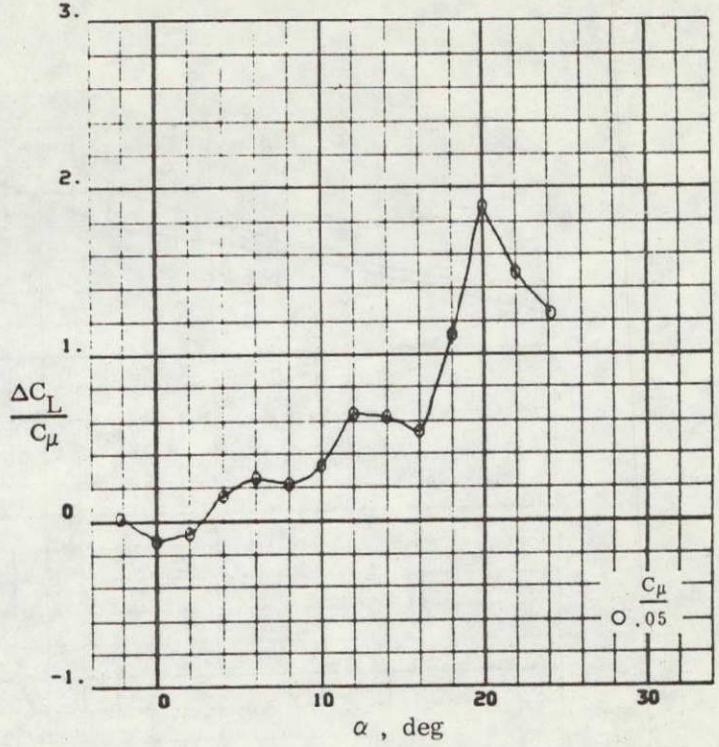

(b) M = 0.7

FIGURE 2.10. EFFECT OF α AND C_μ ON LIFT AUGMENTATION RATIO OF CONFIGURATION WITH HORIZONTAL TAIL (W1N1H)

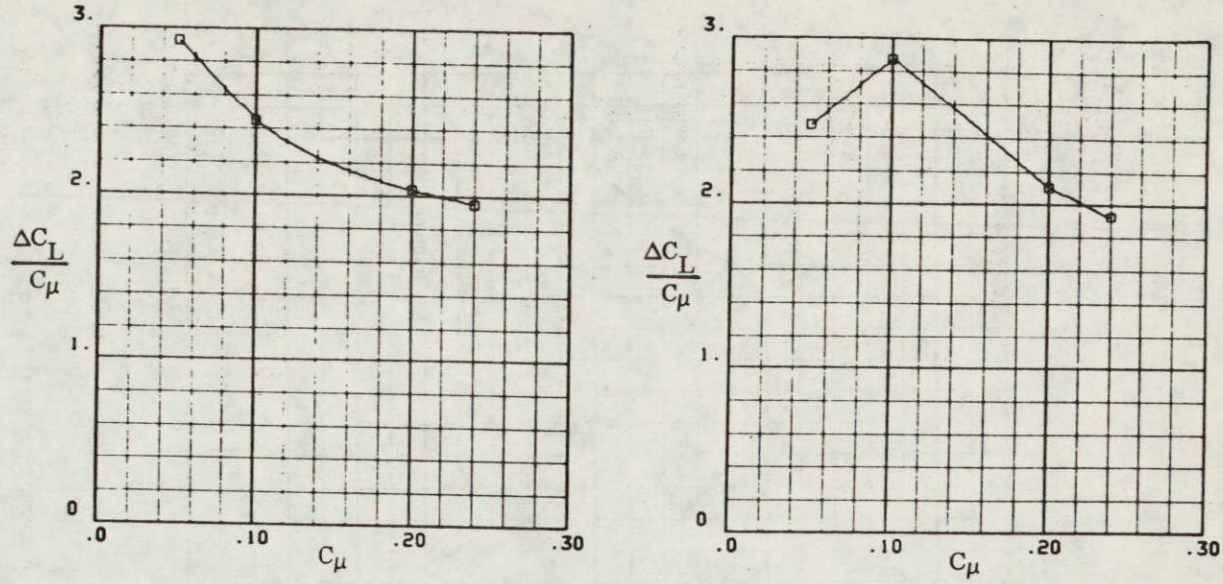

(a) W1N1 (b) W2N1

FIGURE 2.11. EFFECT OF C_μ ON LIFT AUGMENTATION RATIO AT $\alpha = 22°$ (M = 0.3)

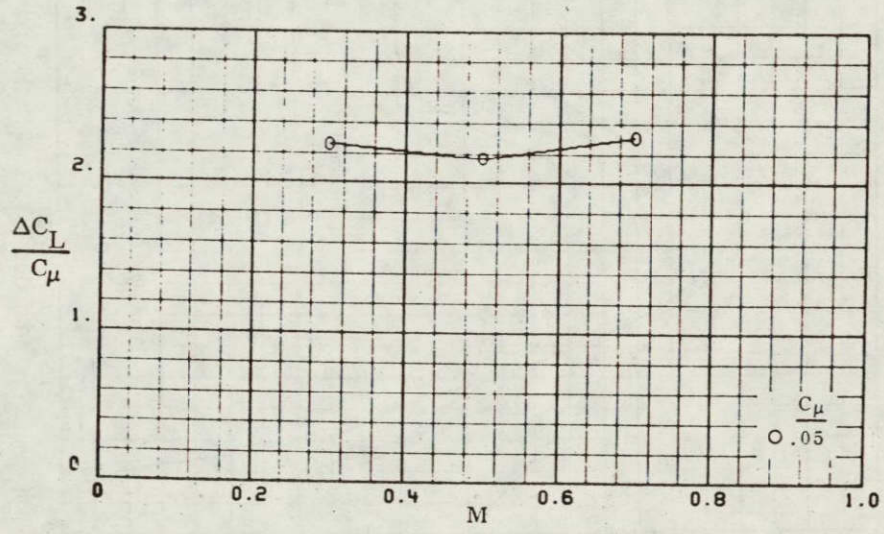

FIGURE 2.12. EFFECT OF MACH NUMBER ON LIFT AUGMENTATION RATIO AT $\alpha = 20°$

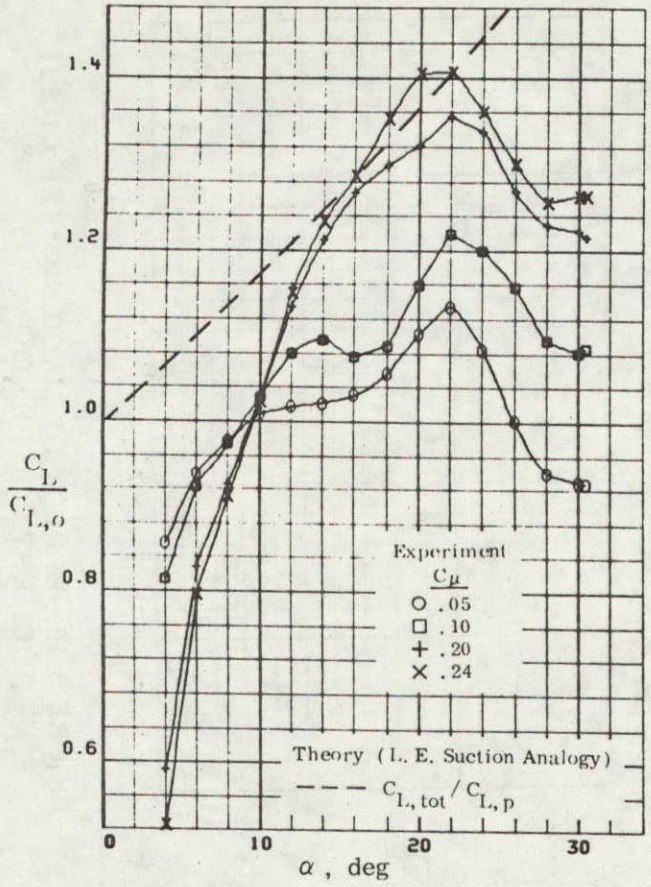

(a) M = 0.3

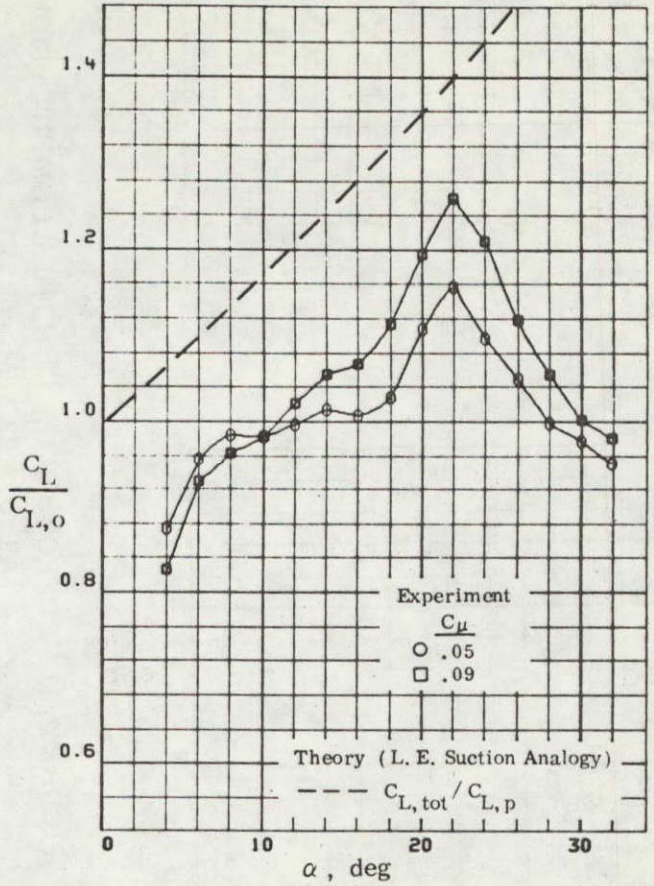

(b) M = 0.5

FIGURE 2.13. EFFECT OF α AND C_μ ON LIFT EFFECTIVENESS

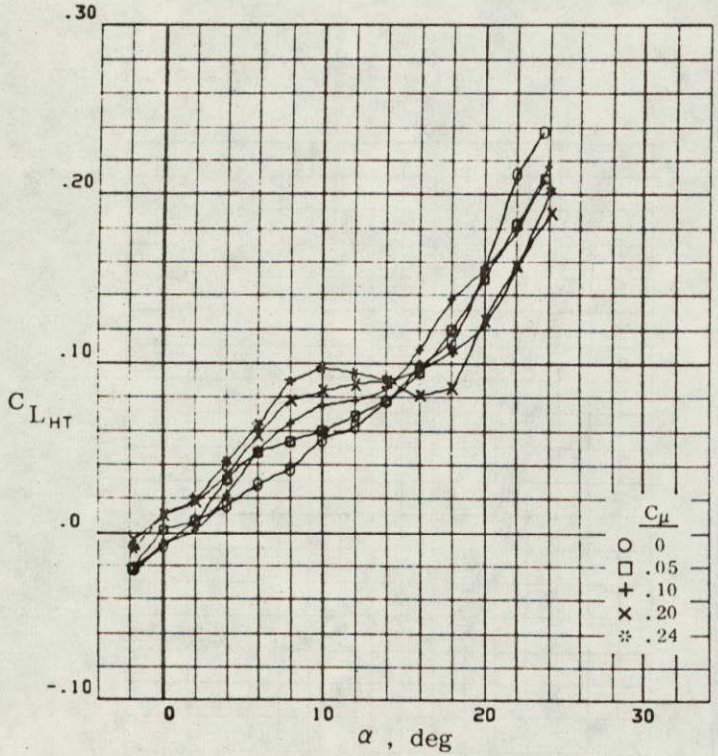

(a) M = 0.3

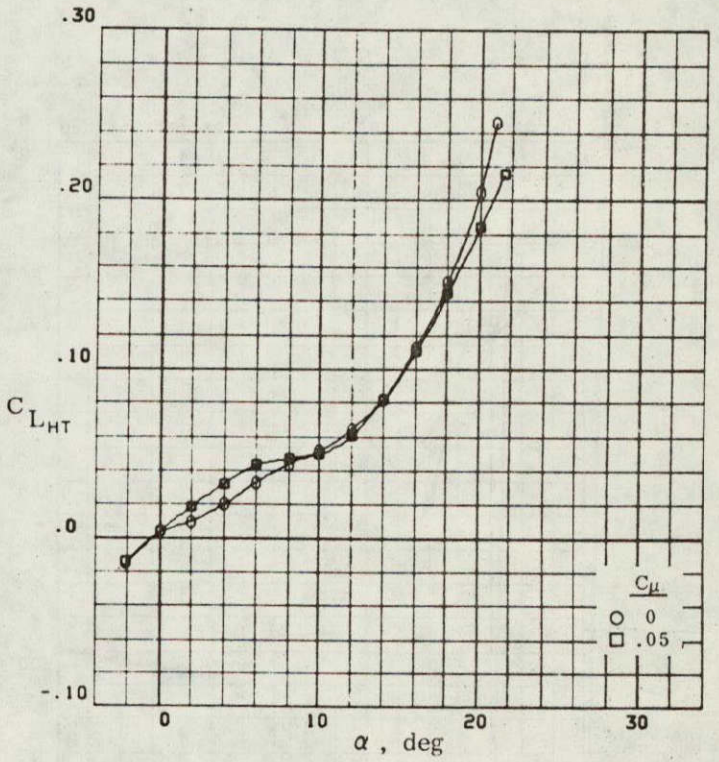

(b) M = 0.7

FIGURE 2.14. EFFECT OF α AND C_μ ON LIFT CONTRIBUTION OF HORIZONTAL TAIL

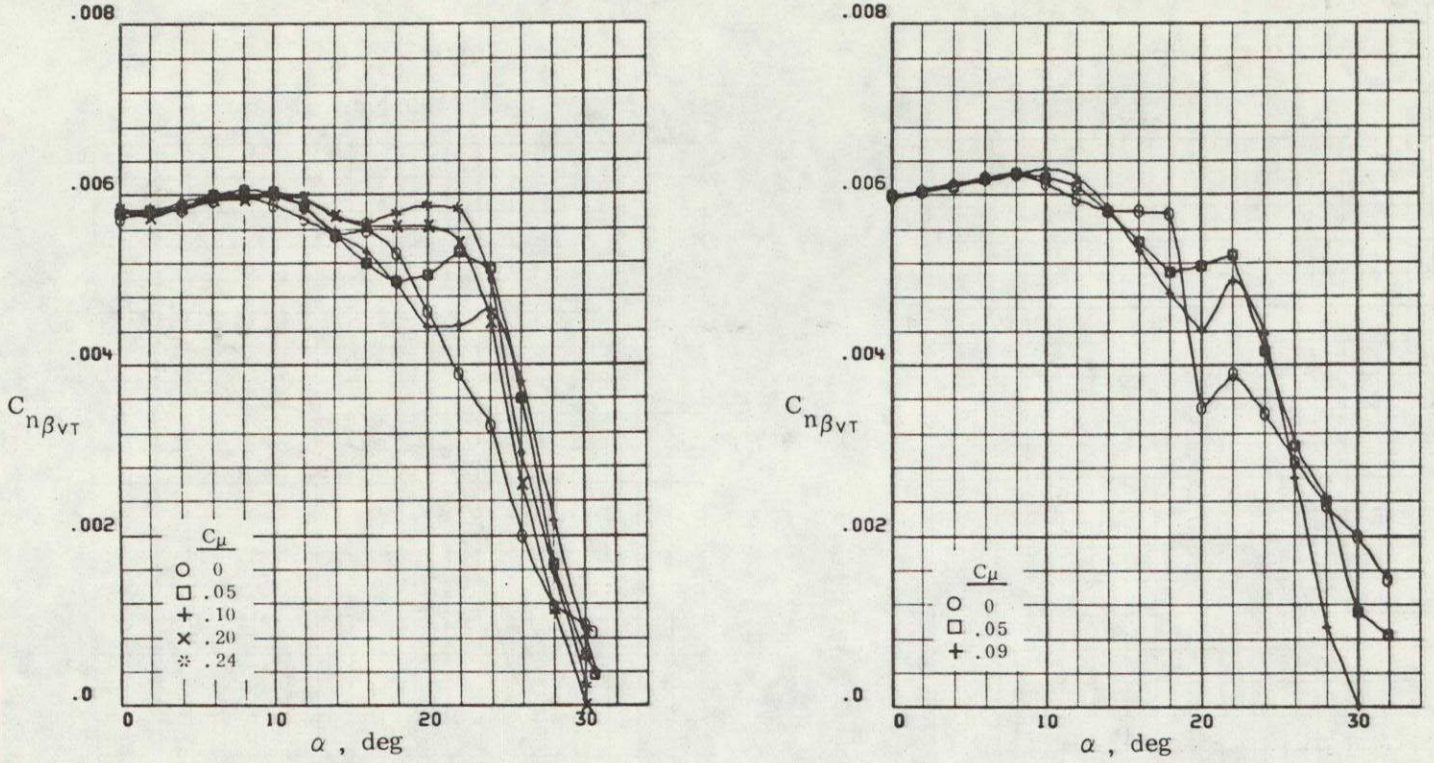

(a) M = 0.3

(b) M = 0.5

FIGURE 2.15. INFLUENCE OF FLUID STRAKE ON VERTICAL TAIL EFFECTIVENESS

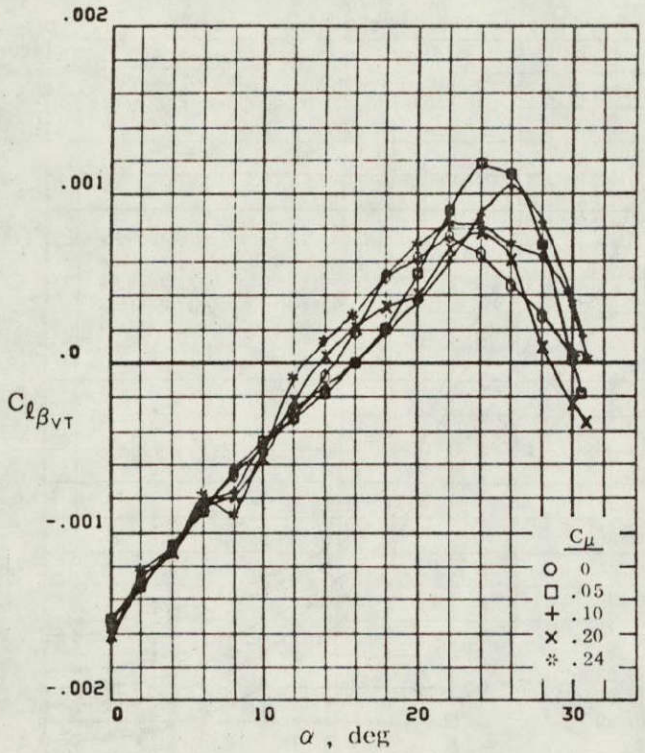

(a) M = 0.3

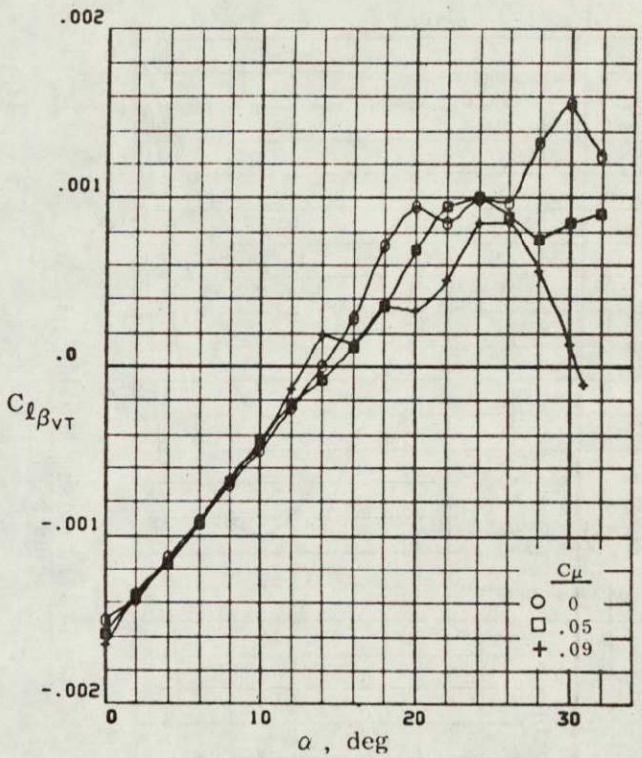

(b) M = 0.5

FIGURE 2.16. INFLUENCE OF FLUID STRAKE ON EFFECTIVE DIHEDRAL DUE TO VERTICAL TAIL

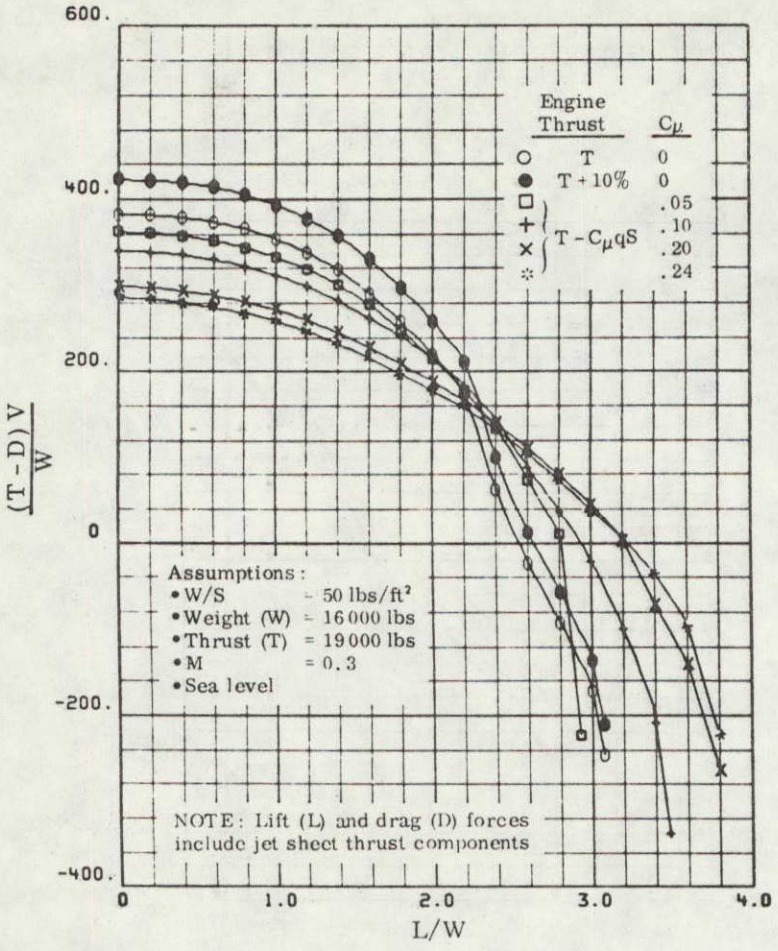

FIGURE 2.17. EFFECT OF FLUID STRAKE ON SPECIFIC EXCESS POWER

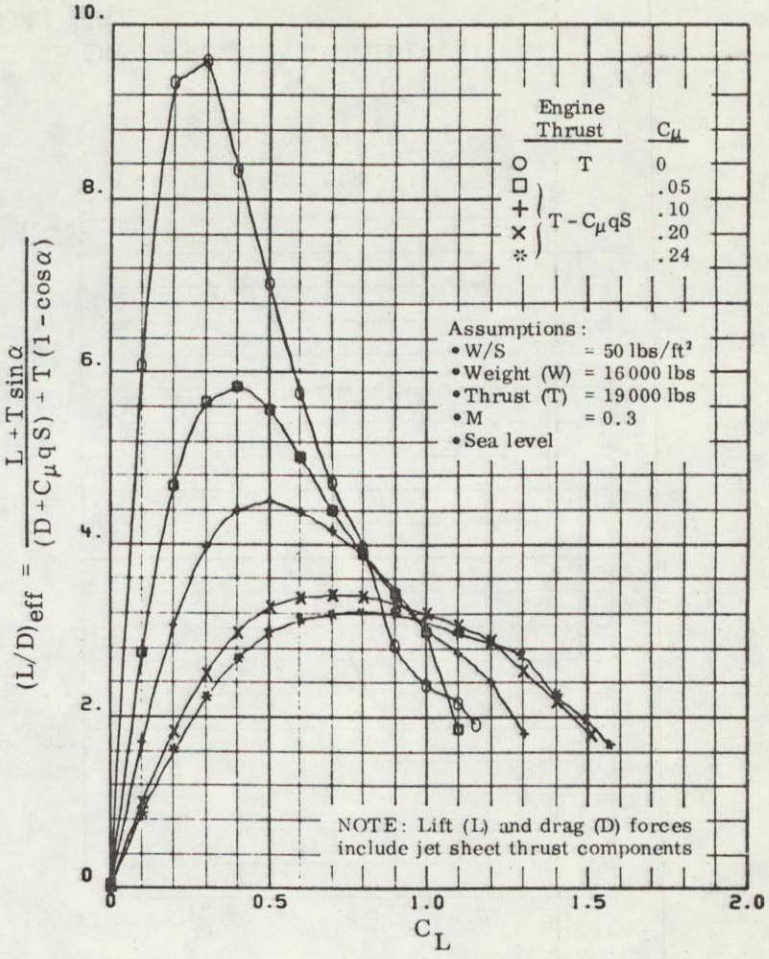

FIGURE 2.18. EFFECT OF FLUID STRAKE ON L/D

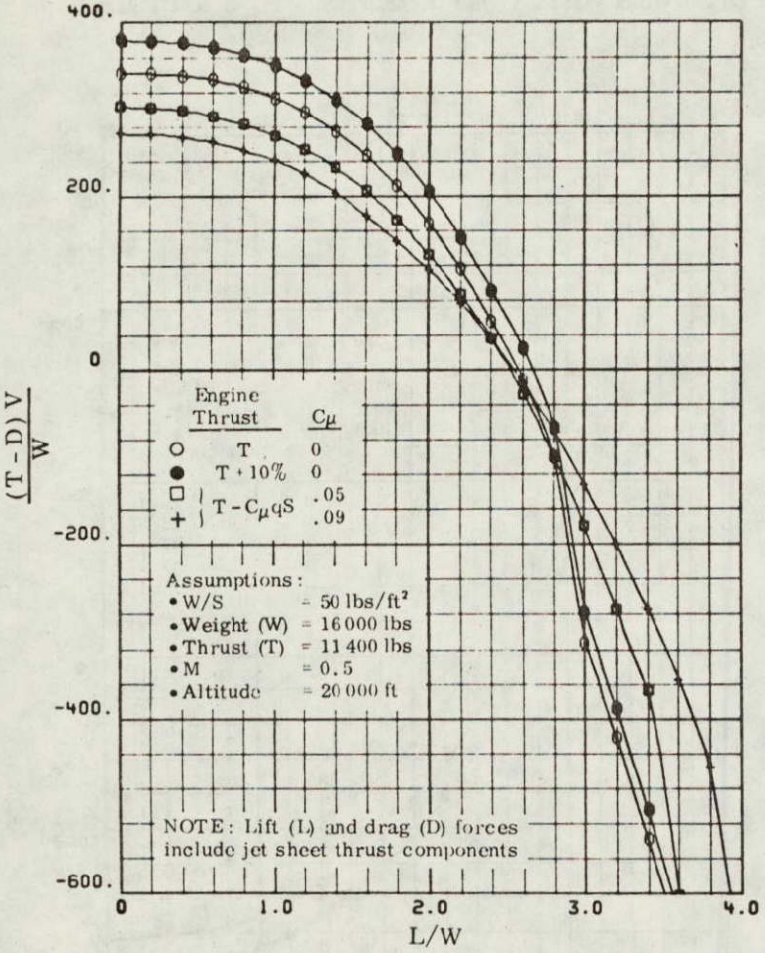

FIGURE 2.19. EFFECT OF FLUID STRAKE ON SPECIFIC EXCESS POWER

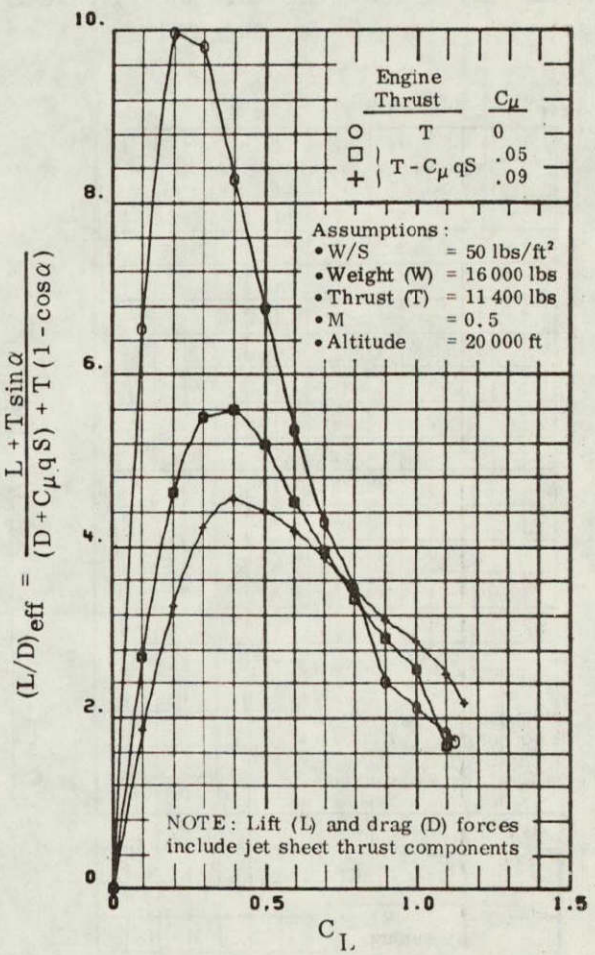

FIGURE 2.20. EFFECT OF FLUID STRAKE ON L/D

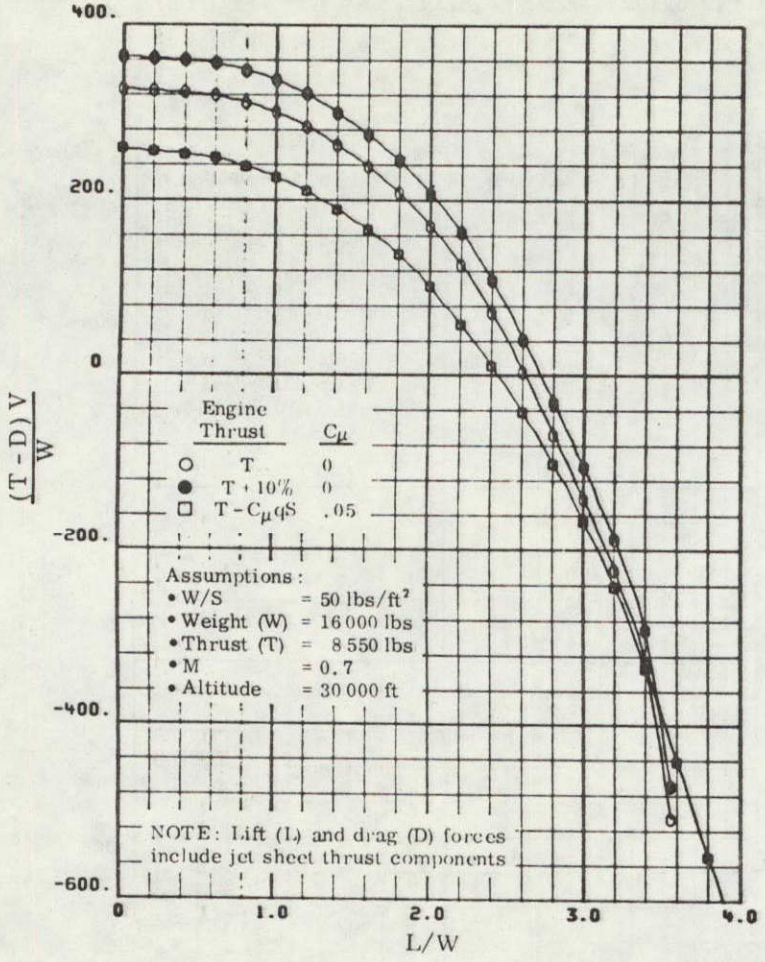

FIGURE 2.21. EFFECT OF FLUID STRAKE ON SPECIFIC EXCESS POWER

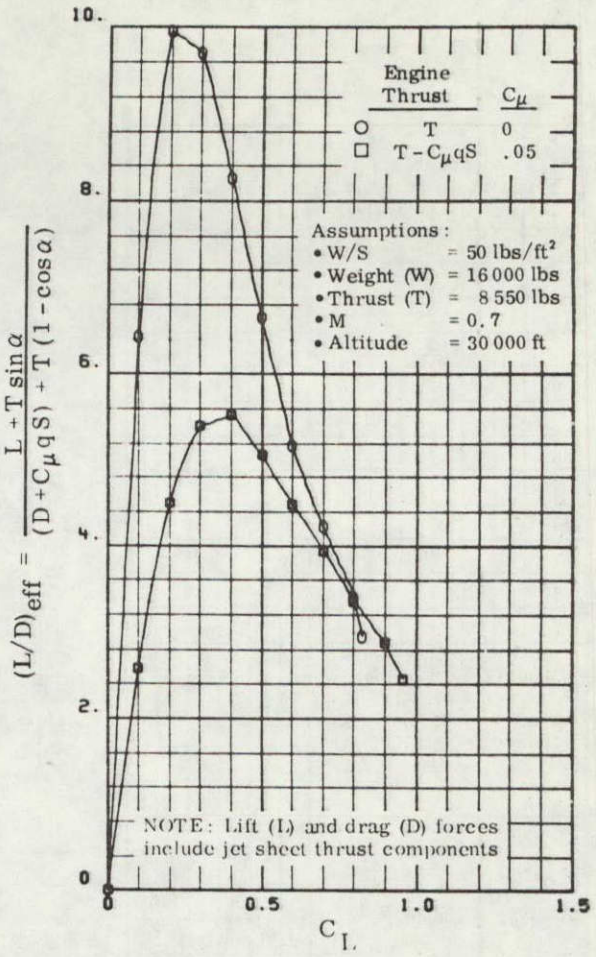

FIGURE 2.22. EFFECT OF FLUID STRAKE ON L/D

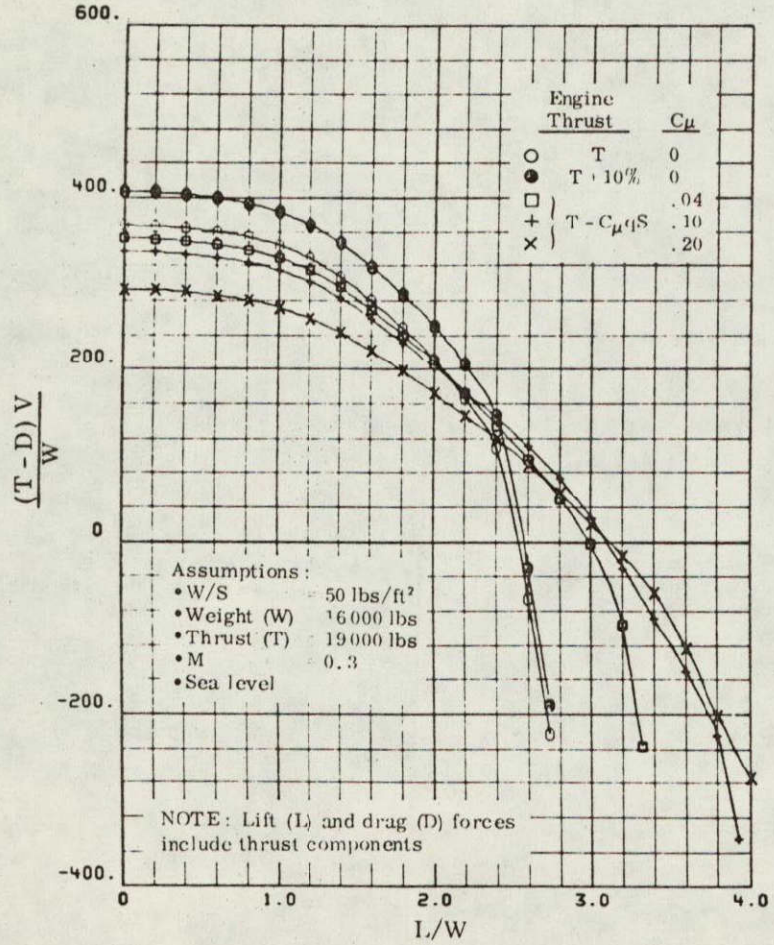

FIGURE 2.23. EFFECT OF SPANWISE BLOWING ON SPECIFIC EXCESS POWER

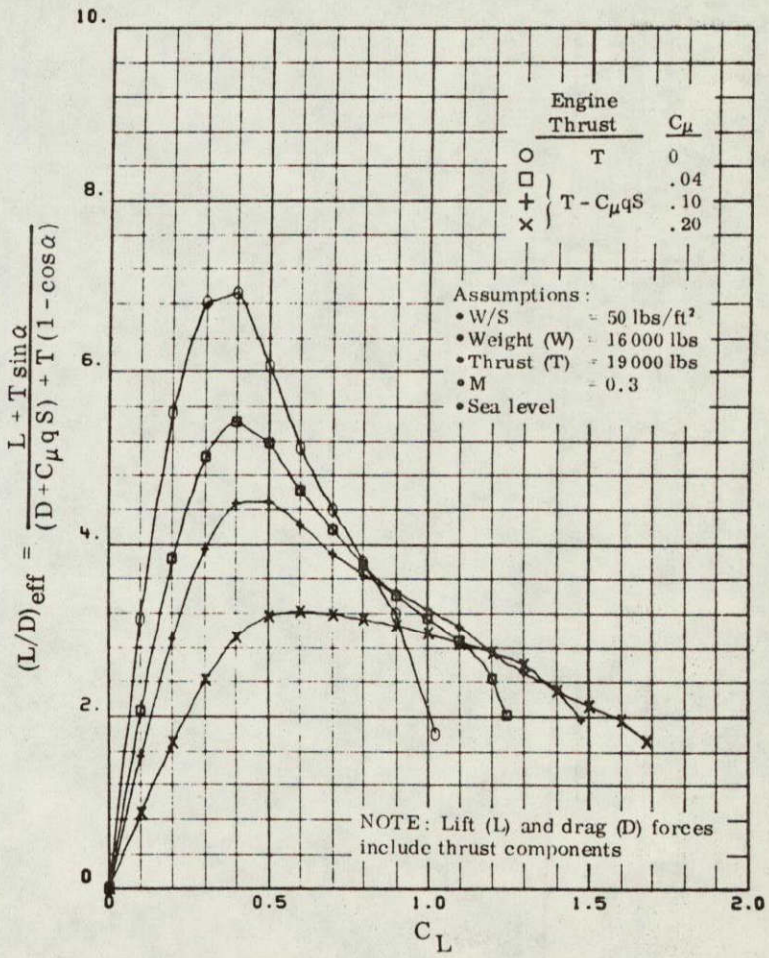

FIGURE 2.24. EFFECT OF SPANWISE BLOWING ON L/D